JPET Fast Forward. Published on June 17, 2014 as DOI: 10.1124/jpet.114.214643

JPET #214643

Vimocin and Vidapin, cyclic KTS peptides, dual antagonists of α1β1/α2β1 integrins with anti-angiogenic activity

Tatjana Momic, Jehoshua Katzehendler, Ofra Benny, Adi Lahiani, Gadi Cohen, Efrat Noy, Hanoch Senderowitz, Johannes A. Eble, Cezary Marcinkiewicz and Philip Lazarovici*

School of Pharmacy Institute for Drug Research, Faculty of Medicine, The Hebrew University of Jerusalem, Jerusalem 91120, Israel (T.M., J.K., O.B., A.L., G.C., P.L.); Department of Bioengineering, College of Engineering, Temple University Philadelphia, PA 19122, USA (C.M.); Department of Chemistry, Bar Ilan University, Ramat-Gan 52900, Israel (E.N., H.S.); Center for Molecular Medicine, Department of Vascular Matrix Biology, Frankfurt University Hospital, Excellence Cluster Cardio-Pulmonary System, 60590 Frankfurt, and Institute for Physiological Chemistry and Pathobiochemistry, University of Münster, 48149 Münster, Germany (J.A.E.);

JPET Fast Forward. Published on June 17, 2014 as DOI: 10.1124/jpet.114.214643
This article has not been copyedited and formatted. The final version may differ from this version.

a) **Running title**: α1β1/α2β1 peptide antagonists with anti-angiogenic activity

b) **Corresponding author**: Prof. Philip Lazarovici; School of Pharmacy Institute for Drug Research, Faculty of Medicine, The Hebrew University of Jerusalem, Jerusalem 91120, Israel; Tel.: +972-2-6758729; Fax: +972-2-6757490; E-Mail: philipl@ekmd.huji.ac.il

c) **Number of the text pages**: 29;

Number of tables: 3;

Number of figures: 12;

Number of references: 63;

Number of words in Abstract: 225;

Number of words in Introduction: 710;

Number of words in Discussion: 1350;

d) **Abbreviations:** Acm, acetamidomethyl;; bFGF, basic fibroblast growth factor; BrdU, bromodeoxyuridine; BSA, bovine serum albumin; CAM, chorioallantoic membrane; CMFDA, 5-chloromethylfluorescein diacetate; DCM, dichloromethane; Df, fractal dimension; DIPEA, *N*,*N*-diisopropylethylamine; DMT, dimethoxytrityl; DTT, dithiothreitol; ECM, extracellular matrix; ELISA, enzyme-linked immunosorbent assay, Fmoc, fluorenylmethyloxycarbonyl; GST, glutathione S-transferase; HAEC, human aortic endothelial cells; HUVEC, human umbilical vein endothelial cells; HBSS, Hank's Balanced Salt Solution; HBTU, 2-(1*H*-benzotriazole-1yl)-1,1,3,3-tetramethyluronium hexafluorophosphate; HOBt, 1-hydroxybenzo-triazole; iv, intravenously; LDH, lactate dehydrogenase; MD, molecular dynamics; NAD, nicotinamide adenine dinucleotide; NADH, nicotinamide adenine dinucleotide reduced form; NMP, N-methyl-2-pyrrolidinone; NMR, nuclear magnetic resonance; NPT, ensemble in which number of atoms,

pressure and temperature are constant; NVT, ensemble in which number of atoms, volume and temperature are constant; OD, optical density; RP-HPLC, reverse-phase high-performance liquid chromatography; TBAF, tetrabutylamonium fluoride; TBS, Tris-buffered saline; TCA, trichloroacetic acid; TFA, trifluoroacetic acid; TIS, triisopropylsilane; Trt, trityl; VEGF, vascular endothelial growth factor;

e) **Recommended section**: Drug Discovery and Translational Medicine

Abstract

Obtustatin and Viperistatin, members of the disintegrin protein family, served as lead compounds for the synthesis of linear and cyclic peptides containing the KTS binding motif. The most active linear peptide, a Viperistatin analog, indicated the importance of Cys^{19} and Cys^{29}, as well as the presence of Arg at position 24 for their biological activity, and was used as the basic sequence for the synthesis of cyclic peptides. Vimocin (Compound 6) and Vidapin (Compound 10), showed a high potency (IC_{50} 0.17 nM) and intermediate efficacy (20% and 40%) in inhibition of adhesion of α1/α2 integrin overexpressor cells to respective collagens. Vimocin was more active in inhibition of the wound healing (53%) and corneal micropocket (17%) vascularization, while Vidapin was more potent in inhibition of migration in Matrigel tube formation assay (90%). Both compounds similarly inhibited proliferation (50-90%) of endothelial cells, and angiogenesis induced by VEGF (80%) and glioma (55%) in the chorioallantoic membrane assay. These peptides were not toxic to endothelial cell cultures and caused no acute toxicity upon iv injection in mice, and were stable for 10-30 hours in human serum. The *in vitro* and *in vivo* potency of the peptides are consistent with conformational ensembles and 'bio-active' space shared by Obtustatin and Viperistatin. These findings suggest that Vimocin and Vidapin can serve as a dual α1β1/α2β1 integrin antagonists in anti-angiogenesis and cancer therapy.

Introduction

JPET Fast Forward. Published on June 17, 2014 as DOI: 10.1124/jpet.114.214643
This article has not been copyedited and formatted. The final version may differ from this version.

Integrins are a family of cell surface receptors that play essential roles in eukaryotic cell adhesion and migration. These heterodimeric receptors are composed of two non-covalently linked distinct subunits, α and β, each containing a large extracellular binding domain, a transmembrane region, and a short cytoplasmic domain. Upon binding to ligand the integrins cluster and recruit via their cytoplasmic domain cytoskeletal, adaptor and signaling proteins, eventually forming focal adhesions. These not only anchor the cell to the subjacent extracellular matrix (ECM) protein ligands, but also convey signals into the cell. The two major collagen-binding integrins, α1β1 and α2β1, preferentially bind to collagen type IV and I, respectively (Hynes, 1992). In contrast to other β1 containing integrins, α subunits of collagen-binding integrins contain a unique 200 amino acid-long A-domain that is involved in collagen binding (Leitinger and Hogg, 1999). Studies with α1/α2 integrin A-domain chimeras confirmed a preference for different collagen types (Abair et al., 2008). As such, integrin receptors are central to the etiology and pathology of many diseases, such as cardiovascular (Clemetson and Clemetson, 1998), inflammatory (Apostolaki et al., 2008) and neurodegenerative disorders (Engelhardt and Kappos, 2008). They, therefore, have been actively targeted for drug discovery. Many approaches have been developed, entailing the use of classical small molecules, cyclic peptides and engineered antibodies (Goodman and Picard, 2012). To date, major drug discovery attempts have been focused on several integrins, such as glycoprotein (gp) IIbIIIa, α4bβ1, αvβ3 and LFA-1 (αLβ2) and have produced several registered drugs, targeting directly gpIIbIIIa (abciximab, tirofiban, intrifiban), and α4β1 (natalizumab) (Millard et al., 2011; Goodman and Picard, 2012).

In the past decade, using knock-out animals, the importance of collagen-binding integrins α1β1(Pozzi et al., 2000) and α2β1 (Zhang et al., 2008) in tumor angiogenesis was demonstrated.

JPET Fast Forward. Published on June 17, 2014 as DOI: 10.1124/jpet.114.214643
This article has not been copyedited and formatted. The final version may differ from this version.

Furthermore, important contributions of α1β1 (Chen et al., 2005) and α2β1 (Yoshimura et al., 2009; Ibaragi et al., 2011) in cancer and metastatic processes were revealed. These findings emphasize the role of the α1β1 and α2β1 integrins in angiogenesis and cancer and suggest their importance as targets in drug discovery and translational medicine (Goswami, 2013). However, the discovery of small molecule drugs targeting α1β1 and α2β1 integrins has been modest. In those studies pre-clinical attempts were made to inhibit α1β1 with antibody (Riikonen et al., 1995) and α2β1 with peptides (Ivaska et al., 1999; Raynal et al., 2006; Lambert et al., 2008) and small molecules (Funahashi et al., 2002; Choi et al., 2007) in the search for potential therapy of cardiovascular and inflammatory diseases and cancer.

Snake venom natural toxins such as disintegrins (Marcinkiewicz, 2005) and C-type lectins (Arlinghaus and Eble, 2012) are important pharmacological tools as they inhibit integrins with relative selectivity. The disintegrins Obtustatin, isolated from the venom of *Vipera lebetina obtusa* (Marcinkiewicz et al., 2003), and its more potent natural analog Viperistatin, isolated from the venom of *Vipera xantina palestinae* (Kisiel et al., 2004), containing 41-residue monomeric polypeptides cross-linked by four conserved disulfide bonds, are the shortest snake venom disintegrins described to date (Calvete et al., 2007). They are typical members of the disintegrin family with the characteristic three amino acid KTS motif, which is responsible for their selective binding to α1β1 integrin. These KTS-containing disintegrins bind to α1β1 integrin only, in contrast to RGD disintegrins which block α3β1, α5β1, α8β1, αvβ1, αvβ3 and αIIbβ3 (Ruoslahti, 1996; Calvete et al., 2002). The potency of the KTS disintegrins is strictly dependent on the KTS motif, as mutations of individual amino acids in this motif decreased potency by 10- to 80-fold (Brown et al., 2009). NMR solution structure followed by computer modeling of KTS disintegrins indicate that the KTS motif, like RGD, is present in the loop conformation required

for integrin binding (Moreno-Murciano et al., 2003; Calvete et al., 2007; Brown et al., 2009). Based on these considerations, we used those disintegrins as lead compounds for the synthesis of peptides containing the KTS motif in conformational constraint by cyclization via disulfide bridges.

In the present study we describe the synthesis and modeling of linear and cyclic KTS-containing peptides which inhibited α1β1/α2β1-mediated adhesion and blocked angiogenic activity. Vimocin (Compound 6) and Vidapin (Compound 10) fulfilled basic pharmacological criteria, which can be further exploited for drug development or diagnosis and can serve as a tool for investigations into α1β1/α2β1 biological function.

Materials and Methods

Materials. Collagen IV (from bovine placenta villi) was purchased from Chemicon (Temecula, CA); collagen I (from rat tail) and Matrigel from BD Biosciences (Bedford, MA). 96-well polystyrene plates were obtained from Nunc (Roskilde, Denmark) bovine serum albumin (BSA), Hank's Balanced Salt Solution (HBSS) sulfate, alkaline phosphatase-conjugated anti-rabbit antibody, *p*-nitrophenyl phosphate, human recombinant basic fibroblast growth factor (bFGF) and vascular endothelial growth factor 165 kDa (VEGF) were purchased from Sigma-Aldrich (St. Louis, MO). CellTracker™ Green 5-Chloromethylfluorescein diacetate (CMFDA) was purchased from Invitrogen-Molecular Probes (Eugene, OR,). Rabbit polyclonal antibodies against GST were purchased from Molecular Probes (Nijmegen, The Netherlands). BrdU kit was purchased from Roche (Mannheim, Germany). Fertilized Japanese quail eggs (*Coturnix coturnix japonica)* were purchased from Boyd's Bird Co (Pullman, WA). Lactate Dehydrogenase reagent set was purchased from Pointe Scientific, Inc. (Michigan, USA).

Disintegrins. Viperistatin was obtained from the venom of *Vipera xantina palestinae,* as previously described (Staniszewska et al., 2009). Obtustatin was isolated and purified to homogeneity by two chromatographic steps using HPLC as previously reported (Marcinkiewicz et al., 2003).

C-type lectin protein. Vixapatin was obtained from the venom of *Vipera xantina palestinae* as previously described (Staniszewska et al., 2009). Rhodocetin was purified from *C. rhodostoma* venom as reported (Eble et al., 2001).

Cell lines. Human aortic endothelial cells (HAEC) were kindly provided by Prof. Peter I. Lelkes, Temple University and cultured as previously described (Dolle et al., 2005). Human umbilical vein endothelial cells (HUVEC) were obtained from human umbilical cords from healthy women who underwent normal term pregnancies, as described elsewhere

(Marcinkiewicz et al., 2000).. K562 cells transfected with α1 or α2 integrin subunits (Staniszewska et al., 2009). LN18 human glioma cells were prepared as previously described (Walsh et al., 2012).

Peptide synthesis reagents. All amino acids and Rink resin were purchased from GL Biochem Ltd. (Shanghai, China). *N*,*N*-diisopropylethylamine (DIPEA), 2-(1*H*-benzotriazole-1yl)-1,1,3,3-tetramethyluronium hexafluorophosphate (HBTU) and 1-hydroxybenzo-triazole (HOBt) were purchased from BioLab Ltd. (Jerusalem, Israel). All coupling reagents, chemicals and solvents were purchased from Sigma-Aldrich (Rehovot, Israel).

General procedure for peptide preparation and characterization. The peptides were synthesized on a solid phase by standard fluorenylmethyloxycarbonyl (Fmoc) chemistry. The synthesis was carried out manually on a Rink amide resin using Fmoc-protected amino acids. Coupling was performed for 1h with 4 equivalents of HBTU and 1 equivalent of amino acid in the presence of 4 equivalents of HOBt and 8 equivalents of DIPEA. Fmoc groups were removed with 20% piperidine in N-methyl-2-pyrrolidinone (NMP). Cyclization of the peptides was performed using several approaches, as detailed further for each peptide.

Cleavage from the resin and fully deprotection of peptides was carried out using a mixture of TFA/phenol/H_2O/TIS (88:5:5:2 v/v/v/v) for 3h at room temperature (Fields and Fields, 1993). The resin was filtrated and the peptide was precipitated by addition of cold diethyl ether to the filtrate. The precipitate was separated by centrifugation at 3500 rpm for 10 min, solubilized in water and lyophilized.

Synthesized peptides were purified by preparative reverse-phase high-performance liquid chromatography (RP-HPLC) using a C18 column, with an elution gradient of 0-90% acetonitrile with 0.1% trifluoroacetic in water. Peptide purity was verified by Thermo Scientific Dionex

UltiMate 3000 analytical HPLC. All peptides showed 95% purity, based on the chromatographic peak area displayed at 220 nm. The peptides identities were assessed by electrospray ionization mass spectrometry using a ThermoQuest Finnigan LCQ-Duo in the positive ion mode. The data were processed using ThermoQuest Finnigan's Xcalibur™ Biomass Calculation and Deconvolution softwareMasses found using electrospray ionization mass spectrometry were in the range of standard deviation (0.1% of calculated masses) (Todd 1999). Additionally, structure of Compounds 6 and 10 were confirmed by high resolution electrospray ionization mass spectrometry using a LTQ Orbitrap, Thermo Scientific in the positive ion mode. Generic names of the peptides were presented with asterisk(s) representing amino acids which are involved in cyclization. Amnio acids labeled with the same number of asterisk(s) are interacting and forming the bond.

Compounds 1, 2, 3 and 4. The peptides were synthesized as described in the general procedure. Calculated molecular mass for Compound 1 (CWKTSLTSHYC) is 1328.54, and experimentally found is 1329.67; Calculated molecular mass for Compound 2 (GWKTSLTSHYG) is 1236.35, and experimentally found 1237.67; Calculated molecular mass for Compound 3 (CWKTSRTSHYC) is 1371.56, and experimentally found 1372.63; Calculated molecular mass for Compound 4 (GWKTSRTSHYG) is 1279.38, and experimentally found 1280.23.

Compounds 5 and 6. The peptides were synthesized as described in the general procedure. Disulfide bonds within these peptides were formed by oxidation of the two Cys(Trt) amino acids with 0.1 M iodine/MeOH (Kamber et al., 1980). Calculated molecular mass for Compound 5 (C*WKTSRTSHYC*PLYQG) is 1928.20, and experimentally found 1928.01; calculated molecular mass for Compound 6 (C*WKTSRTSHYC*PLYPG) is 1896.8519, found 1896.8518.

JPET Fast Forward. Published on June 17, 2014 as DOI: 10.1124/jpet.114.214643
This article has not been copyedited and formatted. The final version may differ from this version.

Compounds 7 and 8. Fmoc-Lys(Fmoc)-OH was coupled to a glycine already bound to the resin. Following cleavage of Fmoc by 20% piperidine, the peptides were assembled on the two free amino groups of Lys, to form two parallel peptide chains of identical sequence. The pair of cysteines inserted along each chain, were protected by trityl (Trt) and acetamidomethyl (Acm). A one-pot reaction for selective formation of two inter-chain disulfide bonds was carried out by adding 2 ml of 0.1 M I_2 in dichloromethane (DCM) for 6h (Bullesbach and Schwabe, 1991). This method takes advantage of the difference in the kinetic rates of disulfide bond formation by S-Trt and S-Acm in the presence of iodine in DCM. Whereas the Cys(Trt) disulfide bond was formed by oxidation within a few seconds, formation of the Cys(Acm) disulfide bond occurred after about 2 h. Calculated molecular mass for Compound 7 ((C*WKTSRTSHYC**TGKSD)$_2$K) is 3885.36, and experimentally found: 3885.86; Calculated molecular mass for Compound 8 ((C*WKTSC**RTSHTGKSD)$_2$K) is 3552.96, and experimentally found is 3553.01.

Compound 9. Cyclization of the peptide was carried out in a sequential manner during the elongation step. The five cysteines, at positions 6, 7, 29, 34 and 36, were protected by three distinct groups which were introduced as Cys^{7,34,36}(Trt), Cys^{6}(Acm) and Cys^{29}(StBu). In addition, the peptide sequence included seven lysines, two of which were Lys^{10,19} (Trt) and the one at the terminal position was BocLys^{1}(Fmoc). After the insertion of Cys^{36}(Trt), the Trt group was removed with 3% trichloroacetic acid (TCA) and the free SH group formed was allowed to react with bromoacetic acid to form Cys carboxymethyl thioether. The free carboxylic group was then protected by dimethoxytrityl (DMT), resulting in Cys^{36}(S-CH_2COODMT). Following the introduction of Fmoc-Lys^{19}(Trt) into the assembled sequence, its side chain protecting group and the DMT of Cys^{36}(S-CH_2COODMT) were removed with 3% TCA. The free amino group of the Lys^{19} and the free carboxylic group linked to the Cys^{36} were coupled to form an amide bond, as

JPET Fast Forward. Published on June 17, 2014 as DOI: 10.1124/jpet.114.214643
This article has not been copyedited and formatted. The final version may differ from this version.

described in the general procedure for peptide synthesis. At this stage Cys^{29}(StBu) was transformed into Cys^{29}(CH_2CH_2N=Pht) by reduction with dithiothreitol (DTT), followed by alkylation with bromoethyl phthalimide. The Cys^{34}(Trt) was then converted into Cys^{34}(S-CH_2COODMT) by adding 0.1M iodine in methanol, followed by washing, DTT reduction, and alkylation with bromoacetic acid and DMT esterification. The succeeding cyclization was implemented after the insertion of Lys^{10}(Trt). The Trt and the DMT protecting groups of Lys^{10}(Trt) and Cys^{34}(S-CH_2COODMT), respectively were removed with 3% TCA and the free amine and the carboxylic groups formed were coupled. The next cyclization took place between Cys^{29}(CH_2CH_2N=Pht) and Cys^{7}(S-CH_2COOH). After accessing Cys^{7}(Trt), the trityl group was replaced by a carboxymethyl group, as previously described. The phthalic acid of Cys^{29}(CH_2CH_2N=Pht) was removed by 2M hydrazine hydrate/methanol and the free amine formed was coupled with the free carboxylic group of Cys^{7}(S-CH_2COOH). Subsequent to peptide completion, Cys^{6}(Acm) was transformed into Cys^{6}(S-CH_2COOH) in the same manner as Cys^{34}(Trt), while Acm group was cleaved with 0.1 M iodine in methanol, and the Fmoc protecting group of Boc-Lys^{1}(Fmoc) was cleaved by 1M tetrabutylamonium fluoride (TBAF). The free amino and carboxylic groups formed were coupled to yield the cyclization. Calculated molecular mass for Compound 9 (K*TTGPC*C**RQK***KLKPAGTTK****WKTSRTSHYC**TGKSC***DC****G) is 4251.73, and experimentally found is 4251.96.

Compound 10. The peptide was synthesized as described in the general procedure. The two intra-chain disulfide bonds of Compound 10 were prepared in the same manner as in Compounds 7 and 8. Calculated molecular mass for Compound 10 (C*C**WKTSRTSHYC**TGKSC*G) is 2003.7979, and experimentally found 2003.7977.

Modeling Viperistatin analogs in water. The NMR structure of Obtustatin was downloaded from the PDB (PDB code 1MPZ) (Moreno-Murciano et al., 2003) and its first model was used as a starting point for the molecular dynamics (MD) simulation. All Obtustatin models of the original 1MPZ entry were mutated to Viperistatin (L24R, L38V, P40Q) and minimized. The lowest energy structure (model 16) was used as an initial conformation for the simulation of Viperistatin. This same structure was also used to derive appropriate starting points for the simulations of Compounds 3, 5, 6 and 10, using residues 19-29 for compound 3, residues 19-29 and 37-41 with the mutation V38L for compound 5, residues 19-29 and 37-41 with the mutations V38L and Q40P for compound 6 and residues 18-35 with the mutations T18C and D35G for compound 10. Peptides 5, 6 and 10 were gradually minimized, first by optimizing their disulfide bonds only, then by optimizing all side chains and finally by optimizing the whole structures. Prior to minimization, all structures were prepared using the Prepare Protein Protocol as implemented in Discovery Studio to determine residues protonation states (Accelrys, 2005-2009).

MD simulations were performed using the Gromacs Molecular Dynamics package (Hess, 2007) with the AMBER99SB-ILDN force field (Lindorff-Larsen et al., 2010). Peptides were submerged in TIP3P water (Jorgensen et al., 1983) in a cubic box with an extra extension along each axis of the peptide of 10Å. Ions were added to the solution to make the system electrically neutral. Structures were minimized, equilibrated, first under conditions in which number of atoms, volume and temperature are constant (NVT) for 1 ns and then under conditions in which number of atoms, pressure and temperature are constant (NPT) for an additional 1 ns, and finally simulated under NPT conditions for 1 μs. All simulations were performed at 300K with a time step of 2 fs using the leap-frog algorithm (Hockney et al., 1974). Long range electrostatic

interactions were computed using Particle Mesh Ewald Summation (Essmann et al., 1995). The cutoff for van der Waals and Coulomb interactions was set to 10 Å. Periodic boundary conditions were applied. The LINCS algorithm (Hess et al., 1997) was used to constrain bond lengths.

To assess the similarity of the conformational spaces of two compounds, a matrix termed "contained" was developed based on the percentage of conformations of one compound which are similar (i.e., reside within a pre-defined RMSD cutoff) to at least one of the conformations of the other compound. Contained values were calculated between the designed compounds (Compounds 3, 5, 6 and 10) and the reference compounds (Obtustatin/Viperistatin) using a backbone RMSD cutoff of 2 Å calculated for residues 19-29 and using only the last 400 conformations obtained for each compound. These parameters were selected to allow a comparison between all compounds which share residues 19-29 backbone and to remove the effect of the starting conformations. Similar calculations performed with a 1 Å RMSD threshold mainly resulted in zero percentages.

Cell adhesion assay. The assay was carried out as described previously, with minor modifications (Staniszewska et al., 2009). The day before the experiment each well of a 96-well plate was coated with 10 µg/ml collagen I or 1 µg/ml collagen IV in 0.02 M acetic acid and incubated overnight at 4°C. Thereafter non-specific binding was blocked by incubating the wells with 1% (w/v) bovine serum albumin (BSA) in Hank's Balanced Salt Solution (HBSS) containing 5 mM $MgCl_2$, at room temperature for 1 h before use. The cells were labeled by incubation with 12.5 µM 5-chloromethylfluorescein diacetate (CMFDA) in HBSS without 1% BSA at 37°C for 30 min. The labeled cells were then centrifuged at 1000 rpm and washed twice with HBSS containing 1% BSA to remove excess CMFDA. Labeled cells (1×10^5 cells/well)

JPET Fast Forward. Published on June 17, 2014 as DOI: 10.1124/jpet.114.214643
This article has not been copyedited and formatted. The final version may differ from this version.

were added to each well in the presence or absence of peptide and incubated at 37°C for 60 min. In the presence of peptide, cells were added to the well after prior incubation with peptide for 30 min at 37°C. Unbound cells were removed by washing the wells three times with 1% (w/v) BSA in HBSS, and bound cells were lysed by the addition of 0.5% Triton X-100 (diluted in DDW). The fluorescence in each well was quantified with a SPECTRAFluor Plus plate reader (Tecan), at λ_{ex} = 485 nm and λ_{em} = 530 nm. To determine the number of adhered cells from the fluorescence values, a standard curve was generated by serial dilution of known numbers of CMFDA-labeled cells.

GST-α1A/GST-α2A binding to type IV/I collagens binding assay. Inhibition ELISA was performed as described previously (Eble and Tuckwell, 2003), with the following modifications: CB3 (collagen IV fragment) or collagen I was immobilized overnight at 4°C on a microtiter plate at 10 μg/ml in TBS/$MgCl_2$ (50 mM Tris-HCl, 150 mM NaCl, and 2 mM $MgCl_2$, pH 7.4) and 0.1 M acetic acid, respectively. After blocking the plate with 1% BSA in TBS/$MgCl_2$, the GST-tagged α1A/GST-tagged α2A domain was allowed to bind to type IV collagen/collagen I in the presence or absence of different peptides for 2 h at room temperature. The bound GST-α1A/GST-α2A domain was fixed for 10 min with 2.5% glutaraldehyde in HEPES buffer (50 mM HEPES, 150 mM NaCl, and 2 mM $MgCl_2$, and 1 mM $MnCl_2$, pH 7.4). The bound GST-α1A/GST-α2A was quantified with rabbit polyclonal antibodies against GST, followed by alkaline phosphatase-conjugated anti-rabbit antibody, which served as the primary and secondary antibodies, respectively, each diluted in 1% BSA in TBS/$MgCl_2$. The conversion of *p*-nitrophenyl phosphate was measured at 405 nm in an ELISA reader Bio Tek, (Bad Friedrichshall, Germany). Nonspecific binding was assessed by binding of GST-α1A/GST-α2A to BSA or of α1β1/α2β1 integrin to collagen IV/collagen I in the presence of 10 mM EDTA.

Cell proliferation assay. HAEC and HUVEC proliferation was assessed using a BrdU kit according to the manufacturer's instructions.

Cell migration assay. HUVEC migration was measured using wound healing assay (Lecht et al., 2010). In brief, 1 x 10^{-6} cells/well were added to 24-well culture plate. Upon formation of a confluent monolayer, cell migration was initiated by scratching HUVEC monolayer with small sterile pipette tip, thus generating a cell-free area (wound) of ~1 mm width. The wounded cells were washed three times with 1% FCS supplemented EGM-2 medium and the photos of the wounds at time 0 h were taken. Thereafter, culture medium were changed to 2% FBS medium as cell migration stimulator, in the presence or absence of synthetic peptides (50 μg/ml) or Obtustatin (5 μg/ml) and the cultures were allowed to migrate for 24 h. At the end of migration experiment, another set of photos was taken, of the same regions. Images were analyzed using ImageJ software. In order to assess cell migration at the wound edge and to calculate the area covered by migrating cells, the cell-free areas of the wounds at 24 h post-wounding were subtracted from the area of the wounds at 0 h time point and calculated as a percentage of untreated (control) cultures (Lecht et al., 2010).

Human aortic endothelial cell tube formation in the Matrigel assay. The assay was performed using a 96-well plate coated with growth factor reduced Matrigel. Briefly, 1x10^4 HAEC or HUVEC per well (in complete EMB-2 media or 2% FBS) were added in the presence or absence of the peptides, and the plate was incubated overnight at 37^{o}C in 5% CO_2. Images were captured under an inverted microscope (Olympus IX81), with 35 x magnification (Momic et al., 2012a).

JPET Fast Forward. Published on June 17, 2014 as DOI: 10.1124/jpet.114.214643
This article has not been copyedited and formatted. The final version may differ from this version.

Angiogenesis in the chorioallantoic membrane (CAM) quail embryonic model. The assay of VEGF-induced and tumor-induced angiogenesis in the quail embryonic CAM system was performed as described previously (Lazarovici et al., 2006).

Fertilized Japanese quail eggs (*Coturnix coturnix japonica)* were cleaned with ethanol, and maintained at 37°C until embryonic day 3 in an incubator without CO_2. The shells were then opened with a razor blade. Using minced sterile scissor, the contents were transferred to 6-well tissue culture plates and returned to the 37°C incubator. At embryonic day 7, the compounds, were applied under sterile conditions to the surface of the CAM and after 24 h the effect on the aortic tree was evaluated. The embryos were divided into experimental groups, each containing at least 10 embryos. The control group was treated with vehicle (PBS).

In the experiments using LN18-induced tumors under the CAM, LN18 glioma cells (1×10^7/50µl) were injected at day 7 under the CAM and tumor-induced angiogenesis was measured at day 12. At the end of the experiment the embryos were fixed with 5 ml of pre-warmed 2% gluteraldehyde, 4% paraformaldehyde in PBS for 48 h at room temperature. Membranes with and without tumor were dissected and mounted on glass slides for evaluation of the fractal dimension (D_f). The area of CAM selected as a square for analysis of the vascularization ratio, was localized as previously described or, in the case of the tumor induced-angiogenesis, in the site opposite to the tumor on the membrane. For example, if the tumor developed in the right corner of the CAM, the vascularization tree for analysis was framed in the left corner of the membrane (Lazarovici et al., 2006).

Corneal micropocket assay. The corneal micropocket assay was performed as previously detailed (Benny et al., 2008). In brief, pellet containing 80 ng carrier-free recombinant human bFGF or 160 ng VEGF (R&D Systems) were implanted into micropockets

which were created in the cornea of anesthetized mice. Mice were treated daily by eye drops (8 mg/ml) for 5 days, and then the vascular growth area was measured using a slit lamp. The area of neovascularization was calculated as vessel area calculated as vessel length measured from the limbus and clock hours around the cornea, using the following equation: Vessel area (mm2)=(π x clock hours x vessel length (mm) x 0.2 mm).

Stability of Compounds 3, 6 and 10 in human serum. One ml of RPMI supplemented with 25% (v/v) of human serum was introduced into a 1.5 ml Eppendorf tube and temperature-equilibrated at 37^{o}C for 15 min before adding 5 µl of peptide stock solution to make a final peptide concentration of 50 µg/ml. The initial time was recorded and at known intervals 100 µl of the reaction solution was removed and added to 200 µl of 96% ethanol to precipitate serum proteins. The sample was cooled at 4 ^{o}C for 15 min and then centrifuged at 18000 g for 2 min to precipitate serum proteins. The supernatant was then applied to a C-18 column for separation by RP-HPLC. A linear gradient from 100% buffer A (0.1% TFA in water), to 50-50% buffer A and buffer B (0.1% TFA in acetonitrile), was applied for over 30 min. The flow rate was 1 ml/min and absorbance was detected at 220 nm (Jenssen and Aspmo, 2008).

Cell death assay. Cell death was measured by the release of lactate dehydrogenase (LDH) into the medium, in the absence and presence of different concentrations of Compound 10, using Lactate dehydrogenase reagent. H_2O_2 was used as positive control. LDH activity was determined spectrophotometrically at 340 nm by following the rate of conversion of oxidized nicotinamide adenine dinucleotide (NAD) to the reduced form of (NADH). LDH release was expressed as the optical density (OD) units. Each experiment was performed two times (n = 6).

Toxicity to mice. Experiments with and animal care were approved by the Committee of Ethics of The Hebrew University and were performed in strict accordance with the Guide for the

Care and Use of Laboratory Animals published by the US National Institutes of Health. A 50 mg/kg quantity of Compounds 6 and 10, in 0.2 ml were injected intravenously (iv) in male C57BL/6 mice and SABRA-M mice (n=3) and they were monitored for three consecutive weeks. The animals were examined for autonomic symptoms by measuring salivation, urinary delivery, pupillary constriction, hart rate, blood pressure, and hair contraction. Neurotoxicity was evaluated by general locomotors activity of the animals in the cage and the ability of the peptide-injected mice to maintain balance and motor coordination by crossing 3 cm, 2 cm and 1 cm width balance beam. Occurrence of either flaccid or spastic paralysis of the legs were also measured. Blood samples were taken from control and peptide-injected mice after 10 hours from injection and submitted from hematocrit and biochemical analysis.

Statistics. Student's t test and ANOVA were used to determine the significance of the differences between the various treatments compared with the control groups. $p \leq 0.05$ was considered significant.

Results

Synthesis of linear peptides. In the first approach, linear Obtustatin and Viperistatin peptide analogs (Fig. 1A) containing the KTS motif (Table 1) were synthesized and their biological activity was investigated by an *in vitro* adhesion assay with K562 cells overexpressing the α1 integrin subunit, using the ligand collagen IV. The peptides with the highest anti-adhesive activity are presented in Table 1. The most active peptide was Compound 3, Viperistatin analog. Compound 1, Obtustatin analog, the sequence of which differs from Compound 3 only by one amino acid at position 24 where Leu^{24}→Arg^{24}, had six fold decreased activity. This suggests that the positively charged side chain of Arg form a better productive interaction with residues within the ligand-binding pocket of the α1β1 integrin (Brown et al., 2009) than the alkyl chain of Leu. In addition, we showed that the two Cys of Compound 3, at the carboxy and amino termini of the sequence had a strong impact on its potency. Upon exchanging the two terminal Cys with two Gly, the α1-mediated anti-adhesive activity of Compounds 4 and 2 decreased significantly by 35-fold and 7-fold, respectively, indicating their important role in binding α1β1 integrin.

Synthesis of cyclic peptides. In the second approach, conformationally constrained cyclic sequences containing the KTS motif were prepared. In the first group (Fig. 1B) we synthesized two cyclic peptides with one intradisulfide bridge between Cys^{19} and Cys^{29} i.e., Compounds 5 and 6, the structure of which differs by only one amino acid Gln^{33}→Pro^{33}, respectively. To generate new analogs, a second group was synthesized (Compounds 7 and 8) (Fig. 1C), represented by two peptides with double intercyclization. The cyclization was achieved by the formation of two disulfide bonds between two identical strand sequences containing the modified 19-35 Viperistatin sequence. In both peptides Cys^{34} was omitted. In Compound 8, an additional modification was done by exchanging the position of Cys from

JPET Fast Forward. Published on June 17, 2014 as DOI: 10.1124/jpet.114.214643
This article has not been copyedited and formatted. The final version may differ from this version.

position 29, to position 24. In both peptides cyclization was achieved by linking Cys of identical protecting groups residing on two identical peptide strands. Two interdisulfide bonds were formed between $Cys^{19,19}$ and $Cys^{29,29}$ of Compound 7, and between $Cys^{19,19}$ and $Cys^{24,24}$ in Compound 8 (Fig. 1C). The third group of peptides is presented by Compounds 9 and 10 (Fig. 1D). The structure of Compound 9 is a modified Viperistatin sequence, where the amino acids at positions 37-40 are eliminated. The peptide is characterized by four intrastrand amide bonds between $Lys^{1}$and Cys^{6}, Cys^{7} and Cys^{29}, Lys^{10} and Cys^{34}, and Lys^{19} and Cys^{36}. Compound 10 includes the original Viperistatin 19-34 sequence and one additional Cys at position 18. Its two intradisulfide bonds involved are between Cys^{18} and Cys^{34} and Cys^{19} and Cys^{29}.

Potency and efficacy of Viperistatin analogs in the adhesion assays. In the cellular adhesion assay, the inhibitory effect of all the synthesized peptides was first tested using α1-K562 transfectants. To measure the potency and efficacy of Viperistatin analogs, we performed dose-response experiments in a range of physiological concentrations between 0.1 nM-100 nM, using collagen IV-coated plates. As expected, Viperistatin blocked α1-mediated cell adhesion to collagen IV (Fig. 2A) with an apparent IC_{50} of 0.6 nM and 100% efficacy (Table 2). Compounds 5 and 6 with one intracyclization were characterized by very similar IC_{50} values of 0.20 and 0.17 nM, respectively and an equal efficacy of 20% (Fig. 2A, Table 2). Apparently, the substitution at position 33, of Gln in Compound 5 by Pro in Compound 6 did not affect the activity. Compounds 7 and 8, with intercyclization, were characterized by an identical IC_{50} of 0.15 nM and an efficacy of 25% (Fig. 2B, Table 2). Compounds 9 and 10 with intracyclization were characterized by an identical IC_{50} of 0.17 nM and an efficacy of 40% (Fig. 2C, Table 2). All the synthesized peptides were characterized by increased potency compared with Viperistatin (Figure 2A-C, Table 2). By contrast, inter- or intra-cyclization of the peptides resulted in reduced

JPET Fast Forward. Published on June 17, 2014 as DOI: 10.1124/jpet.114.214643
This article has not been copyedited and formatted. The final version may differ from this version.

efficacy, to a level of 20% for Compounds 5 and 6, 25% for Compounds 7 and 8 and 40% for Compounds 9 and 10, vs Viperistatin (Figure 2A-C, Table 2). In conclusion, cyclization significantly increased the potency but reduced the efficacy of the synthesized peptides, in comparison with Viperistatin.

To test the specificity of the Viperistatin analogs towards the α1β1 and α2β1 integrins we used α2-K562 transfectants and measured the potency and efficacy of the analogs in the same range of concentrations, using collagen I-coated plates and Vixapatin, an α2 selective C-type lectin protein (Arlinghaus and Eble, 2012), as positive control. Vixapatin generated a dose-response inhibitory effect on α2 mediated adhesion, with an apparent IC_{50} of 3 nM and an efficacy of 100% (Figure 2D and Table2). Viperistatin analogs showed a high potency of inhibition, with an apparent IC_{50} in the range of 0.12-0.25 nM and a very low efficacy in the range of 10-30% (Figure 2 D-F, Table 2). These findings indicate that the synthesized peptides interfered with α1β1 and α2β1 integrin-mediated adhesion.

A cell-free assay was performed to assess whether the synthesized peptides directly interact with the A domain of α1 or α2. For this purpose, Viperistatin and Rhodocetin, another C-type lectin protein selective for α2β1 integrin, as well as Compounds 3, 5-10, were incubated together with the GST-linked A domains, and allowed to bind to the immobilized collagen I or CB3 (collagen IV fragment). The amount of the bound recombinant A domain, provided information on the inhibitory potential and biochemical recognition ability of the peptides (Fig. 3). Similarly to Obtustatin (Marcinkiewicz et al., 2003), Viperistatin did not inhibit binding of the GST- α1A domain to collagen at a concentrations of 1 μM (Fig 3. A). However, at a high concentrations (range 2-1000 μM), Compounds 6 and 10, dose-dependently inhibited binding of GST-α1A by 50% (Fig. 3B). This finding suggests that Viperistatin affects α1 integrins outside

of the A-domain, most probably by conformational changes, whereas Compounds 6 and 10 recognize with low potency a motif in the A domain. In the experiments with the GST-α2A domain at 1 μM concentration, a similar lack of inhibition was observed (Fig. 3C). However, in the range of concentrations between 0.01 and 1.0 μM, as previously reported (Eble and Tuckwell, 2003), Rhodocetin inhibited binding of the GST- α2A domain to collagen I in a dose-dependent manner (Fig. 3D). Surprisingly, Compounds 6 and 10 increased the binding of GST-α2A to collagen I in a dose-dependent manner, most probably by a conformational change. These results may suggest that Viperistatin analogs affect α1A and α2A integrin domains at non-physiological concentrations, but the mechanism requires further investigation.

Modeling Viperistatin analogs in water. To evaluate the effect of differences in amino acids composition and number of disulfide bonds on peptides conformation, molecular dynamic (MD) simulations were performed. MD simulations were performed for each of the reference compounds, Viperistatin and Obtustatin and for the compounds 3, 5, 6 and 10 as described in the Methods section. The selection of these Compounds was done based on the results we obtained in all the biological experiments presented in this work. 500 snapshots were collected in each case (see supplementary material). The last 400 snapshots of Viperistatin and Obtustatin were superimposed using the backbone of residues 4-18 and 30-36 (Moreno-Murciano et al., 2003) and are presented as "sausage" plots (Koradi et al., 1996) in Figure 4A and Figure 4B, respectively. These plots show a mean structure with atom-wise error bars indicated by the thickness of the sausage. Results for Viperistatin (Fig. 4A) show that the KTS loop (in pink) region is more mobile relative to the other parts of the peptide. Results of Obtustatin (Fig. 4B) show that the KTS loop (in pink) and the C-terminal regions are also more mobile relative to the other parts of the peptide. To qualitatively address the conformational space sampled by the

designed compounds we present for each one 10 superimposed, evenly spread, conformations collected from the last 800 ns of its trajectory. Compound 3 samples the conformational space extensively (Fig. 4C). Compounds 5 and 6 are also quite flexible, though to a lesser extent (Fig. 4D and Fig. 4E, respectively). Compound 10 is clearly the least flexible one (Fig. 4F). The trend observed for Compounds 3, 5, 6 and 10 is in accordance with their structures, namely, larger numbers of disulfide bonds restrict the conformational space of the designed compounds.

Furthermore, we examined the degree of similarity between the conformational spaces sampled by the designed compounds and the reference compounds, Viperistatin and Odtustatin to investigate the assumption that conformational similarity translates into similar activities (Fig. 5, Table 3). For each compound we calculated the percentage of its conformations which are "contained" within the conformational space of a reference compound and complementary the percentages of the reference compounds' conformations "contained" within the conformational space of that compound. The first value (on the left, Fig. 5) estimates the fraction of time a compound spends in the conformational space of the reference compounds (i.e., in conformations similar to those of the reference compounds) while the second value (on the right, Fig. 5) estimates what part of the conformational space of the reference compound is sampled. The two reference compounds, Viperistatin and Obtustatin, sample the conformational spaces of each other rather extensively with Viperistatin having 79.6% of its conformations close to Obtustatin and Obtustatin having 68.8% of its conformations close to Viperistatin. This similarity is in accordance with the high anti-adhesive activity of both compounds. Compound 3 has relatively low "contained" percentages in the conformational ensembles of the reference compounds 11.5% and 17.0% for Obtustatin and Viperistatin, respectively and high "contained" percentages of the reference compounds 79.6% and 96.8% of Obtustain and Viperistain,

respectively in its ensemble (Table 3). The corresponding numbers for Compound 5 are 30.4%, 40.1%, 34.9% and 88% (Table 3), those for Compound 6 are 3.7%, 10.0%, 50.6% and 19.0% (Table 3) and those for Compound 10 are 94.5% (for both Obtustain and Viperistain), 64.3% and 68.1% (Table 3). These data indicate that Compound 3 samples most of the conformational space of the reference compounds, but only for a short fraction of the time. Compound 5 samples less of the conformational space of the reference compounds, but for longer periods of time. Compound 10 samples quite a large fraction of the conformational space of the reference compounds throughout most of the simulation. The fraction of time Compounds 3, 5 and 10 spend in the conformational space of the reference compounds are in accordance with their anti-adhesive activity. This confirms the assumption that conformational similarity translates into similar activity. Compound 6 deviates from this pattern and apparently its disulfide bond locks its structure in a set of conformations remote from those characteristic by the reference compounds for most of the time. It is interesting to note that although Compounds 5 and 6 differ only in one residue (Gln^{40} in compound 5 and Pro^{40} in Compound 6, similar to Viperistatin and Obtustatin, respectively) they show significant differences in their conformational ensembles. While the conformational ensemble of Compound 5 is relatively similar to those of the reference compounds, that of Compound 6 is clearly different. It is likely that the combination of the rigid Pro residue with the disulfide bonds locks this peptide in a unique set of conformations.

Viperistatin analogs inhibit proliferation and migration of endothelial cells. To further characterize the effect of the peptides on endothelial function, we screened their influence on HUVEC and HAEC proliferation, using the BrdU assay (Fig. 6). Similarly to Obtustatin, a 50 µg of Compounds 6 and 10, inhibited proliferation of HAEC by 90%. Compounds 3, 7, 8 and 9 had no effect (Fig. 6A). The effect of Compound 6 on the inhibition of HUVEC and HAEC

proliferation was 50-90% (Fig. 6A,B). Compound 10, like Obtustatin, completely inhibited the proliferation of both cell lines. These results indicate the angiostatic effect of Viperistatin analog Compounds 6 and 10 on endothelial cells.

In another approach, we characterized the effect of 50 μg of Compounds 6 and 10, which were the most active in inhibition of endothelial cells proliferation, on HUVEC migration using wound healing assay (Figure 7). While in untreated cells (control) 100% of wound closing was measured, Obtustatin blocked by 100% wound closing. Interestingly, Compound 10 blocked by 26% and Compound 6 to a higher extent, inhibited by 53% wound closing. These results also indicate anti-angiogenic effects of these compounds on HUVEC.

Viperistatin analogs inhibit tube formation in the Matrigel assay. To investigate the ability of the peptides to inhibit tube formation by HAEC and HUVEC, the Matrigel angiogenesis assay was performed. Treatment for 14 h with 100 μg Obtustatin, as well as with Compounds 6 and 10, completely inhibited tube formation (Fig. 8). These results indicate the angiostatic effect on endothelial cells of Viperistatin analog Compounds 6 and 10.

Viperistatin analogs inhibit angiogenesis in the CAM assay. In the first approach, the effect of Viperistatin analogs on VEGF-induced angiogenesis in the CAM quail embryonic model was measured. The binary images of the mid-arterial endpoint CAM fragments showed a significant overgrowth of small capillaries after 24 h of treatment with VEGF in comparison with control vehicle-treated embryos (Fig. 9, panel – VEGF, Control). At 200 μg per embryo, Compounds 6 and 10 significantly (80%) inhibited VEGF-induced capillary formation, as found with 20 μg Obtustatin per embryo (Fig. 9).

In the second approach, the effect of the Viperistatin analogs on angiogenesis induced by glioblastoma tumor cells was estimated. LN18 glioma cells were injected into the shell-less

JPET Fast Forward. Published on June 17, 2014 as DOI: 10.1124/jpet.114.214643
This article has not been copyedited and formatted. The final version may differ from this version.

embryonic CAM system and the effect of the Viperistatin analogs on mid-arterial capillary sprouting was measured (Fig. 10A). LN18 glioma tumor induced a significant increase in angiogenesis (Fig. 10A, panel), expressed by an increase in fractal dimension (Df) values from 1.106 to 1.162, 50% greater than that of the control. Treatment with 100 μg Compound 6 reduced LN18-induced-angiogenic effect by 50%, very similar to the effect caused by the same amount of Compound 10 (Fig. 10A,B). Those results characterized Compounds 6 and 10 as anti-angiogenic compounds.

Viperistatin analogs inhibit angiogenesis in corneal micropocket assay. The anti-angiogenic properties of Compounds 6 and 10 were evaluated *in vivo* with corneal micropocket assay (Benny et al., 2008). After 5 days of treatment with 8 mg/kg of Compounds 6 and 10, the anti-angiogenic effect was measured with 80 ng bFGF induced angiogenesis in the eyes of treated mice compared to untreated mice (control) (Figure 11, upper panel). Quantification of angiogenesis area (Figure 11, lower pannel) showed 20 ± 5% inhibition of angiogenesis with Compound 6, compared to control ($p=0.05$, $n=10$). Compound 10 did not show statistically significant inhibition in this assay. Similar peptide inhibitory results were obtained with 200 ng VEGF induced angiogenesis in the cornea (data not shown).

Viperistatin analogs stability in human serum. To investigate the effects of the peptide cyclization on proteolytic susceptibility, the degradation of the intact peptides incubated in human serum at 37^{o}C was followed by RP-HPLC. Incubations were done for different periods of time and results were presented in Figure 10. The linear peptide, Compound 3 was degraded with half-live of 3 h. In contrast to linear peptide, cyclization of peptides prolonged their stability. Compound 6 containing one cyclization was completely degraded after 24 hours with half-life of

JPET Fast Forward. Published on June 17, 2014 as DOI: 10.1124/jpet.114.214643
This article has not been copyedited and formatted. The final version may differ from this version.

10 hours. Compound 10 with double cyclization showed a more complex degradation behavior, and 50% of the starting peptide amount was preserved for 30 hours in human serum.

Safety of Viperistatin analogs. First, to verify that the anti-angiogenic effect of Viperistatin analogs is not due to toxicity towards endothelial cells, Compounds 6 and 10 (100 μM) were incubated with HUVEC and HAEC for seven days and the amount of LDH release in the medium was estimated. No significant release of LDH over the control (10±5%) was measured for all cultures up to seven days of treatment, indicating lack of necrotic cell death (data not shown). Considering that IC_{50} of these compounds for inhibition of cell adhesion is 0.17 nM, we can estimate a therapeutic index *in vitro* of 1000, indicating high safety for endothelial cells.

Secondly, to investigate the safety of Viperistatin analogs in mice, we injected iv for three consecutive weeks male mice with a dose of 50 mg/kg of Compounds 6 and 10. Acute tolerability was observed. At injection of this high dose of 50 mg/kg body weight, the mice didn't suffered from visible weakness and/or exhaustion. No paralysis, altered motor activity, or irregular behavior were observed in mice treated with Compounds 6 and 10, suggesting lack of neurotoxicity. Cutaneous hematomas around the injection or at distant locations site within 24 h after injection have not been either observed. Furthermore, no mice sudden deaths occurred within 24 h after the injection or during the 3 weeks of observation. The blood of mice injected with Compounds 6 and 10, after 10 h was submitted for hematological and biochemical analysis. The values for white blood cells, red blood cells and platelets counts were in the normal range of 6-15x10^3/μl, 7-12x10^6/μl and 200-450x10^3/μl, respectively for mice injected with Compounds 6 and 10 similarly with the values obtained for control mice. Additional evidence on the lack of hemorrhage or anemic conditions were indicated by similar hematocrit value in the range of 35-

45% and mean corpuscular hemoglobin of 11.1-12.7 pg/mice, between Compounds 6 and 10 injected mice compared to control mice. Lack of lymphopenia, monocytopenia and granulocytopenia were indicated by similar values in the range of 20-40%, 3-5%, 7-13%, respectively, between Compounds 6 and 10 injected mice compared to control mice. Alkaline phosphatase and lactate dehydrogenase values were in the range of 100-214 U/L and 1000-2400 U/L, respectively, between Compounds 6 and 10 injected mice compared to control mice, suggesting no toxic effects to liver and other tissues.

Discussion

We describe the synthesis, modeling and characterization of Viperistatin analogs that inhibit α1β1/α2β1 integrin-mediated cell adhesion and angiogenic activity. These analogs represent the first attempt to generate KTS peptides using Viperistatin/Obtustatin as lead compounds. All the synthesized cyclic peptides were characterized by sub-nano molar potency, intermediate efficacy of binding, dual antagonism of α1 and α2 integrins, different stability in human serum, safety to endothelial cells and mice, and differential angiostatic effects. Summarizing all experiments, we suggest that Compounds 6 and 10, which we named Vimocin and Vidapin, respectively, can serve as optimal cyclic peptides for future research and development of α1β1/α2β1 receptor antagonists.

One of the classical approaches for generating pharmacophores of pharmaceutical importance utilizing snake venom-derived disintegrins is to produce linear peptides and, subsequently, cyclic peptides (Dennis et al., 1990; Millard et al., 2011). Consistent with this approach, in the present study, using the structure of Viperistatin/Obtustatin as a template, we first synthesized linear peptides with the KTS sequence and investigated their inhibitory potency

in an adhesion cellular assay. Compound 3 was the most active linear peptide, although its potency was extremely low, compared with that of Viperistatin. The other, less potent linear analogs of Viperistatin (Table 1), emphasize the important role of Cys at the flanking N and C terminal ends, as well as the important role of Arg at position 24, for their biological activity, as previously reported for Viperistatin and Obtustatin (Brown et al., 2009; Momic et al., 2012b).

Based on these findings, as well as the consideration that the integrin-binding loop supports the correct conformational presentation of the KTS sequence to α1β1 integrins (Brown et al., 2009), in the second approach we synthesized cyclic Viperistatin analogs. The Compound 3 linear sequence served as a basic structure for the cyclic peptides. Using single, double and tetra, inter- or intra-cyclization, we generated peptides of various sizes and structural constraints. The data we obtained in adhesion assay indicate that the number and type of cyclization had no significant effect on the potency of the cyclic compounds investigated, albeit the cyclization dramatically increased the potency as compared with that of Compound 3. Although all the cyclic peptides showed reduced efficacy of binding in comparison with Viperistatin, multiple intra-cyclization conferred 40% efficacy of Compounds 9 and 10. The results we obtained by computation studies showed, as expected, an opposite correlation between the number of disulfide bonds and the conformational flexibility of the different compounds, with more bonds conferring conformational rigidity (Figure 4) as well as stability (Figure 12). Based on the analysis of the conformational ensembles, the conformational space sampled by Compound 10 is the most similar to those of the reference peptides, Obtustatin and Viperistatin, being the least flexible among the modeled peptides. Compound 6 was more flexible than Compound 10. This observation lends some credit to the hypothesis that active compounds have similar conformational ensembles. This hypothesis is supported by conformation-activity studies of

potent RGD peptides (Gurrath et al., 1992), as well as studies on the size and shape of the integrin-binding loop as a determinant for conferring integrin specificity on cyclic RGD peptides with a known conformation (McLane et al., 1996). Our present findings indicating the increased potency of Viperistatin cyclic anologs, compared with that of linear peptides, are supported by previous studies in which cyclic RGD analogs showed a higher potency than their linear analogs (Pierschbacher and Ruoslahti, 1987; Wong et al., 1998). In addition to the A domain, the α subunits of the integrin receptors contain a variety of other motifs, such as: extracellular β-propeller, thigh, genu, calf-1, calf-2, trans-membrane and cytoplasmic (Xiong et al., 2001) to which these analogs may bind allosterically resulting in an antagonistic effect on adhesion. Furthermore, experiments with recombinant α1 A- and α2 A-domains suggest that Compounds 6 and 10 interact with α integrin sequences located outside the A domain. This may suggest that partial overlap with the conformational space of the reference compounds is sufficient for activity of Compounds 6 and 10, which in turn implies that only part of the conformational space of the unbound (i.e., in solution) reference compounds is occupied by these compounds in their integrin bound state. This "bio-active" space is apparently shared by Compounds 10 and 6 but to a lesser extent by Compounds 5 and 3. These possibilities will be clarified in future experiments of characterizing the interactions between Viperistatin analogs with whole α1 and α2 recombinant integrin receptor proteins.

As both the α1 and α2 integrins provide critical support for physiological and/or tumor angiogenesis (Senger et al., 2002), we characterized the effect of Viperistatin analogs in several *in vitro* angiogenic assays, such as endothelial cell proliferation and migration and tube formation in Matrigel, and *in vivo* capillary formation in the CAM assay and corneal micropocket assay. Here we report that the novel Compounds 6 and 10 efficiently inhibited

endothelial cell proliferation and migration in wound healing assay, tube formation in Matrigel, as well as VEGF and glioma- induced angiogenesis in the CAM assay. However, in the *in vitro* wound healing assay using HUVEC Compound 6 was found more potent that Compound 10, and *in vivo*, in mice corneal micropocket assay, mainly Compound 6 was found active. These different effects may be related to the different stability profiles of the peptides (Figure 12), or their pharmacokinetic properties in *in vivo* assays. Furthermore, differences in anti-angiogenic properties between Compound 6 and 10 obtained can be attributed to the differences in the assays used. Moreover, angiogenesis is not the same in different tissues and the cornea is naturally avascular (Staton et al., 2009). It is also known that anti-angiogenic compounds, which have efficacy *in vitro*, may not show any activity *in vivo* and vice versa, with some compounds showing little efficacy *in vitro* having strong activity *in vivo* (Liekens et al., 2001). Although Compounds 6 and 10 efficacy of binding was lower than that of their natural lead structures, these findings were anticipated, as we previously found that the natural compound α1 antagonists Viperistatin (Staniszewska et al., 2009) and Obtustatin (Marcinkiewicz et al., 2003) and the α2 antagonist Vixapatin (Momic et al., 2012a) are angiogenic inhibitors. So far, inhibition of angiogenesis by integrin antagonism has been focused mostly on integrins αvβ3 and αvβ5 which serve as receptors for the extracellular matrix proteins fibronectin, vitronectin, and fibrinogen that contain an RGD motif (Cheresh, 1987). The peptides described in our paper were designed based on the structure of the α1β1 integrin-inhibiting Viperistatin. The integrin α1β1 binds collagen in an RGD-independent manner. To our knowledge, Viperistatin is among the first highly selective and potent disintegrins to inhibit α1β1 integrin binding to collagen. The integrin α2β1 is closely related to α1β1 integrin and binds collagen similarly in an RGD-independent manner. Standing far apart from the RGD-dependent integrins, these two collagen-binding

integrins have an overlapping ligand binding specificity. Hence, it is pharmacologically more challenging to test the selectivity of peptides towards α1β1 integrin vs. the very similar α2β1 integrin. The original K562 cells used in the present experiments as control, express only α5β1 integrin (Järvinen et al., 1993). In our hands, their binding to fibronectin coated microtiter plates was not affected by Compounds 6 and 10 and therefore the possibility that these compounds inhibit α5β1 is less plausible. Our findings further point to the involvement of α1/α2 integrins in angiogenesis, consistent with the phenotype of reduced vascularity in α1 and α2 knock-out mice (Pozzi et al., 2000; Zhang et al., 2008).

In summary, the present study describes the synthesis of small, cyclic, KTS peptides and dual antagonists of the α1β1/α2β1 integrins. Compound 6 named Vimocin and Compound 10 named Vidapin are characterized by a high potency and an intermediate efficacy in α1β1 integrin binding, a conformational, tridimensional organization in water similar to Viperistatin and Obtustatin, as well as anti-angiogenic activities. These compounds were characterized by $t_{1/2}$ of 12 and 30 hours, respectively in human serum and were not toxic to endothelial cells in culture and safe upon iv injection in mice. We suggest that these compounds may serve as candidates for drug development in therapy of angiogenesis disorders and cancer.

Acknowledgments

We would like to thank Dr Keren Ettinger for technical help, Mrs Zahava Cohen for help with art work, Dr. Alexander G Alexandrovich and Dr. Victoria Trembovler for help with animal experiments. We are grateful to Prof. Robert D'Amato for allowing as using his facilities for

doing cornea micropocket assay. Prof. Dan Gibson and Dr Raji Raveendran for the help with analytical HPLC analysis.

Authorship contributions

Participated in research Design: Tatjana Momic, Jehoshua Katzehendler, Ofra Benny, Johannes A. Eble, Cezary Marcinkiewicz and Philip Lazarovici

Conducted experiments: Tatjana Momic, Jehoshua Katzehendler, Ofra Benny, Adi Lahiani, Gadi Cohen, Efrat Noy, Johannes A. Eble, Cezary Marcinkiewicz

Contributed new reagents or analytical tool: Efrat Noy, Hanoch Senderowitz, Ofra Benny, Johannes A. Eble, Cezary Marcinkiewicz

Performed data analysis: Tatjana Momic, Jehoshua Katzehendler, Ofra Benny, Efrat Noy, Hanoch Senderowitz, Johannes A. Eble, Cezary Marcinkiewicz and Philip Lazarovici

Wrote or contributed to the writing of the manuscript: Tatjana Momic, Ofra Benny, Efrat Noy, Hanoch Senderowitz, Johannes A. Eble, Cezary Marcinkiewicz and Philip Lazarovici

JPET Fast Forward. Published on June 17, 2014 as DOI: 10.1124/jpet.114.214643
This article has not been copyedited and formatted. The final version may differ from this version.

References

Abair TD, Sundaramoorthy M, Chen D, Heino J, Ivaska J, Hudson BG, Sanders CR, Pozzi A and Zent R (2008) Cross-talk between integrins a1b1 and a2b1 in renal epithelial cells. *Exp Cell Res* **314**:3593-3604.

Accelrys (2005-2009) Discovery Studio Modeling Environment, in, Accelrys Software Inc., San Diego.

Apostolaki M, Manoloukos M, Roulis M, Wurbel M-A, Muller W, Papadakis KA, Kontoyiannis DL, Malissen B and Kollias G (2008) Role of a7 integrin and the chemokine/chemokine receptor pair CCL25/CCR9 in modeled TNF-dependent Crohn's disease. *Gastroenterology* **134**:2025-2035.

Arlinghaus FT and Eble JA (2012) C-type lectin-like proteins from snake venoms. *Toxicon* **60**:512-519.

Benny O, Fainaru O, Adini A, Cassiola F, Bazinet L, Adini I, Pravda E, Nahmias Y, Koirala S, Corfas G, D'Amato RJ and Folkman J (2008) An orally delivered small-molecule formulation with antiangiogenic and anticancer activity. *Nat Biotechnol* **26**:799-807.

Brown MC, Eble JA, Calvete JJ and Marcinkiewicz C (2009) Structural requirements of KTS-disintegrins for inhibition of α1β1 integrin. *Biochem J* **417**:95-101.

Bullesbach EE and Schwabe C (1991) Total synthesis of human relaxin and human relaxin derivatives by solid-phase peptide synthesis and site-directed chain combination. *J Biol Chem* **266**:10754-10761.

Calvete JJ, Fox JW, Agelan A, Niewiarowski S and Marcinkiewicz C (2002) The presence of the WGD motif in CC8 heterodimeric disintegrin increases its inhibitory effect on αIIbβ3, αvβ3, and α5β1integrins. *Biochemistry* **41**:2014-2021.

Calvete JJ, Juárez P and Sanz L (2007) Snake venomics. Strategy and applications. *J Mass Spectrom* **42**:1405-1414.

Chen X, Su Y, Fingleton B, Acuff H, Matrisian LM, Zent R and Pozzi A (2005) Increased plasma MMP9 in integrin α1-null mice enhances lung metastasis of colon carcinoma cells. *Intl J Cancer* **116**:52-61.

Cheresh DA (1987) Human endothelial cells synthesize and express an Arg-Gly-Asp-directed adhesion receptor involved in attachment to fibrinogen and von Willebrand factor. *P Natl Acad Sci USA* **84**:6471-6475.

Choi S, Vilaire G, Marcinkiewicz C, Winkler JD, Bennett JS and DeGrado WF (2007) Small molecule inhibitors of integrin a2b1. *J Med Chem* **50**:5457-5462.

Clemetson KJ and Clemetson JM (1998) Integrins and cardiovascular disease. *Cell Mol Life Sci* **54**:502-513.

Dennis MS, Henzel WJ, Pitti RM, Lipari MT, Napier MA, Deisher TA, Bunting S and Lazarus RA (1990) Platelet glycoprotein IIb-IIIa protein antagonists from snake venoms: evidence for a family of platelet-aggregation inhibitors. *P Natl Acad Sci USA* **87**:2471-2475.

Dolle J-P, Rezvan A, Allen FD, Lazarovici P and Lelkes PI (2005) Nerve growth factor-induced migration of endothelial cells. *J Pharmacol Exp Ther* **315**:1220-1227.

Eble JA, Beermann B, Hinz H-J and Schmidt-Hederich A (2001) α2β1 integrin is not recognized by rhodocytin but is the specific, high affinity target of rhodocetin, an RGD-independent disintegrin and protent inhibitor of cell adhesion to collagen. *J Biol Chem* **276**:12274-12284.

Eble JA and Tuckwell DS (2003) The alpha2beta1 integrin inhibitor rhodocetin binds to the A-domain of the integrin alpha2 subunit proximal to the collagen-binding site. *Biochem J* **376**:77-85.

Engelhardt B and Kappos L (2008) Natalizumab: Targeting α4-integrins in multiple sclerosis. *Neurodegener Dis* **5**:16-22.

Essmann U, Perera L, Berkowitz ML, Darden T, Lee H and Pedersen LG (1995) A smooth particle mesh ewald method. *J Chem Phys* **103**:8577-8593.

Fields CG and Fields GB (1993) Minimization of tryptophan alkylation following 9-fluorenylmethoxycarbonyl solid-phase peptide synthesis. *Tetrahedron Lett.* **34**:6661-6664.

Funahashi Y, Sugi NH, Semba T, Yamamoto Y, Hamaoka S, Tsukahara-Tamai N, Ozawa Y, Tsuruoka A, Nara K, Takahashi K, Okabe T, Kamata J, Owa T, Ueda N, Haneda T, Yonaga M, Yoshimatsu K and Wakabayashi T (2002) Sulfonamide derivative, E7820, is a unique angiogenesis inhibitor suppressing an expression of integrin a2 subunit on endothelium. *Canc Res* **62**:6116-6123.

Goodman SL and Picard M (2012) Integrins as therapeutic targets. *Trends Pharmacol Sci* **33**:405-412.

Goswami S (2013) Importance of integrin receptors in the field of pharmaceutical & medical science. *Adv Biol Chem* **3**:224-252.

Gurrath M, Muller G, Kessler H, Aumailley M and Timpl R (1992) Conformation/activity studies of rationally designed potent anti-adhesive RGD peptides. *Eur J Biochem* **210**:911-921.

Hess B (2007) P-LINCS: A parallel linear constraint solver for molecular simulation. *J Chem Theory Comput* **4**:116-122.

Hess B, Bekker H, Berendsen H and Fraaije J (1997) LINCS: A linear constraint solver for molecular simulations. *J. Comput. Chem.* **18**:1463-1472.

Hockney RW, Goel SP and Eastwood JW (1974) Quiet high-resolution computer models of a plasma. *J Comput Phys* **14**:148-158.

Hynes OR (1992) Integrins: Versatility, modulation, and signaling in cell adhesion. *Cell* **69**:11-25.

Ibaragi S, Shimo T, Hassan NMM, Isowa S, Kurio N, Mandai H, Kodama S and Sasaki A (2011) Induction of MMP-13 expression in bone-metastasizing cancer cells by type I collagen through Integrin α1β1 and α2β1-p38 MAPK signaling. *Anticancer Res* **31**:1307-1313.

Ivaska J, Kapyla J, Pentikainen O, Hoffren A-M, Hermonen J, Huttunen P, Johnson MS and Heino J (1999) A peptide Inhibiting the collagen binding function of integrin a2 domain. *J Biol Chem* **274**:3513-3521.

Järvinen M, Ylänne J and Virtanen I (1993) The effect of differentiation inducers on the integrin expression of K562 erythroleukemia cells. *Cell Biol Int* **17**:399-407.

Jenssen H and Aspmo SI (2008) Serum stability of peptides., in *Peptide-based drug design* (Laszlo O ed) pp 177-186, Humana Press, New York, NY.

Jorgensen WL, Chandrasekhar J, Madura JD, Impey RW and Klein ML (1983) Comparison of simple potential functions for simulating liquid water. *J Chem Phys* **79**:926-935.

Kamber B, Hartmann A, Eisler K, Riniker B, Rink H, Sieber P and Rittel W (1980) The synthesis of cystine peptides by iodine oxidation of S-Trityl-cysteine and S-Acetamidomethyl-cysteine peptides. *Helv Chim Acta* **63**:899-915.

Kisiel DG, Calvete JJ, Katzhendler J, Fertala A, Lazarovici P and Marcinkiewicz C (2004) Structural determinants of the selectivity of KTS-disintegrins for the alpha1beta1 integrin. *FEBS Lett* **577**:478-482.

Koradi R, Billeter M and Wuthrich K (1996) MOLMOL: a program for display and analysis of macromolecular structures. *J Mol Graph* **14**:51-55, 29-32.

Lambert LJ, Bobkov AA, Smith JW and Marassi FM (2008) Competitive Interactions of collagen and a jararhagin-derived disintegrin peptide with the integrin a2-I domain. *J Biol Chem* **283**:16665-16672.

Lazarovici P, Marcinkiewicz C and Lelkes PI (2006) Cross talk between the cardiovascular and nervous systems:neurotrophic effects of vascular endothelial growth factor (VEGF) and angiogenic effects of nerve growth factor (NGF)-implications in drug development. *Curr Pharm Design* **12**:2609-2622.

Lecht S, Arien-Zakay H, Kohan M, Lelkes P and Lazarovici P (2010) Angiostatic effects of K252a, a Trk inhibitor, in murine brain capillary endothelial cells. *Mol Cell Biochem* **339**:201-213.

Leitinger B and Hogg N (1999) Integrin I domains and their function. *Biochem Soc Trans* **27**:826–832.

Liekens S, De Clercq E and Neyts J (2001) Angiogenesis: regulators and clinical applications. *Biochem Pharmacol* **61**:253-270.

Lindorff-Larsen K, Piana S, Palmo K, Maragakis P, Klepeis JL, Dror RO and Shaw DE (2010) Improved side-chain torsion potentials for the Amber ff99SB protein force field. *Proteins* **78**:1950-1958.

Marcinkiewicz C (2005) Functional characteristic of snake venom disintegrins: potential therapeutic implication *Curr Pharm Des* **11**:815-827.

Marcinkiewicz C, Lobb RR, Marcinkiewicz MM, Daniel JL, Smith JB, Dangelmaier C, Weinreb PH, Beacham DA and Niewiarowski S (2000) Isolation and characterization of EMS16, a C-Lectin type protein from Echis multisquamatus venom, a potent and selective inhibitor of the α2β1 integrin *Biochemistry* **39**:9859-9867.

Marcinkiewicz C, Weinreb PH, Calvete JJ, Kisiel DG, Mousa SA, Tuszynski GP and Lobb RR (2003) Obtustatin: a potent selective inhibitor of alpha1beta1 integrin *in vitro* and angiogenesis *in vivo*. *Cancer Res* **63**:2020-2023.

McLane MA, Vijay-Kumar S, Marcinkiewicz C, Calvete JJ and Niewiarowski S (1996) Importance of the structure of the RGD-containing loop in the disintegrins echistatin and eristostatin for recognition of aIIbb3 and avb3 integrins. *FEBS Lett* **391**:139-143.

Millard M, Odde S and Neamati N (2011) Integrin targeted therapeutics. *Theranostics* **1**:154-188.

Momic T, Cohen G, Reich R, Arlinghaus FT, Eble JA, Marcinkiewicz C and Lazarovici P (2012a) Vixapatin (VP12), a C-type lectin-protein from Vipera xantina palestinae venom: Characterization as a novel anti-angiogenic compound. *Toxins* **4**:862-877.

Momic T, Katzhendler J, Marcinkiewicz C, Eble AJ and Lazarovici P (2012b) Medicinal chemistry approach for solid phase synthesis of peptide mimetics of viperistatin disintegrin as lead compounds for α1/α2 integrin receptors in *32nd European Peptide Symposium* (Kokotos G, Constantionou-Kokotou V and Matsoukas J eds) pp 304-305, The European Peptide Society, Athens, Greece.

Moreno-Murciano MP, Monleon D, Marcinkiewcz C, Calvete JJ and Celda B (2003) NMR solution structure of the non-RGD disintegrin obtustatin. *J Mol Biol* **329**:135-145.

Pierschbacher MD and Ruoslahti E (1987) Influence of stereochemistry of the sequence Arg-Gly-Asp-Xaa on binding specificity in cell adhesion. *J Biol Chem* **262**:17294-17298.

Pozzi A, Moberg PE, Miles LA, Wagner S, Soloway P and Gardner HA (2000) Elevated matrix metalloprotease and angiostatin levels in integrin a1 knockout mice cause reduced tumor vascularization. *P Natl Acad Sci USA* **97**:2202-2207.

Raynal N, Hamaia SW, Siljander PR-M, Maddox B, Peachey AR, Fernandez R, Foley LJ, Slatter DA, Jarvis GE and Farndale RW (2006) Use of synthetic peptides to locate novel integrin a2b1-binding motifs in human collagen III. *J Biol Chem* **281**:3821-3831.

Riikonen T, Vihinen P, Potila M, Rettig W and Heino J (1995) Antibody against human a1b1 integrin Inhibits HeLa cell adhesion to laminin and to type I, IV, and V collagens. *Biochem Biophys Res Co* **209**:205-212.

Ruoslahti E (1996) RGD and other recognition sequences for integrins. *Annu Rev Cell Dev Biol* **12**:697-715.

Senger D, R , Perruzzi CA, Streit M, Koteliansky VE, de Fougerolles AR and Detmar M (2002) The α1β1 and α2β1 integrins provide critical support for vascular endothelial growth factor signaling, endothelial cell migration, and tumor angiogenesis. *Am J Pathol* **160**:195-204.

Staniszewska I, Walsh EM, Rothman VL, Gaathon A, Tuszynski GP, Calvete JJ, Lazarovici P and Marcinkiewicz C (2009) Effect of VP12 and viperistatin on inhibition of collagen receptors: dependent melanoma metastasis. *Cancer Biol Ther* **8**:1507-1516.

Staton CA, Reed MWR and Brown NJ (2009) A critical analysis of current in vitro and in vivo angiogenesis assays. *Int J Exp Pathol* **90**:195-221.

Todd JFJ (1991) Recommendations for nomenclature and symbolism for mass spectroscopy. *Pure Appl Chem* 63:1541-1566.

Walsh EM, Kim R, Del Valle L, Weaver M, Sheffield J, Lazarovici P and Marcinkiewicz C (2012) Importance of interaction between nerve growth factor and α9β1 integrin in glial tumor angiogenesis. *Neuro-Oncology* **14**:890-901.

Wong A, Hwang SM, Johanson K, Samanen J, Bennett D, Landvatter SW, Chen W, Heys JR, Ali FE, Ku TW, Bondinell W, Nichols AJ, Powers DA and Stadel JM (1998) Binding of [3H]-SK&F 107260 and [3H]-SB 214857 to purified integrin aIIbb3: Evidence for a common binding site for cyclic Arginyl-Glycinyl-Aspartic acid peptides and nonpeptides. *J Pharmacol Exp Ther* **285**:228-235.

Xiong J-P, Stehle T, Diefenbach B, Zhang R, Dunker R, Scott DL, Joachimiak A, Goodman SL and Arnaout MA (2001) Crystal structure of the extracellular segment of Integrin aVb3. *Science* **294**:339-345.

Yoshimura K, Meckel KF, Laird LS, Chia CY, Park J-J, Olino KL, Tsunedomi R, Harada T, Iizuka N, Hazama S, Kato Y, Keller JW, Thompson JM, Chang F, Romer LH, Jain A, Iacobuzio-Donahue C, Oka M, Pardoll DM and Schulick RD (2009) Integrin α2 mediates selective metastasis to the liver. *Cancer Res* **69**:7320-7328.

Zhang Z, Ramirez NE, Yankeelov TE, Li Z, Ford LE, Qi Y, Pozzi A and Zutter MM (2008) α2β1 integrin expression in the tumor microenvironment enhances tumor angiogenesis in a tumor cell-specific manner. *Blood* **111**:1980-1988.

JPET Fast Forward. Published on June 17, 2014 as DOI: 10.1124/jpet.114.214643
This article has not been copyedited and formatted. The final version may differ from this version.

Footnotes

PL holds The Jacob Gitlin Chair in Physiology and is affiliated and partially supported by The Grass Center for Drug Design and Synthesis of Novel Therapeutics, The Hebrew University of Jerusalem, Israel. The authors greatly appreciate the financial support of the HUJI Intramural Research Funds (P.L.). The Wolfson Foundation for Scientific Research (P.L.), the Sidney Edelstein Foundation (P.L.), Hebrew University Yissum baby seed (P.L.; J.K.), the Israel Ministry of Industry and Commerce, Kamin and the Nofar Programs with TEVA Co. (P.L.; J.K.), The German-Israeli Foundation (GIF- 994-3.9/2008) (P.L.; J.K.; J.A.E.), and Deutsche Forschungsgemenschaft (DFG) through grant SFB/TR 23 project A8 (J.A.E.).

Disclosure

The authors declare no conflicts of interest in this study.

Figure Legends

Figure 1. Cyclic peptide structures.

Figure 2. Inhibitory effect of the peptides on α1 and α2 overexpressor cells adhesion. Dose response curves of the inhibition of (A-C) α1 and (D-F) α2 cell adhesion to respective collagens: Viperistatin and Vixapatin were used as controls. The mean number of adherent cells, ± SD, is derived from three independent experiments.

Figure 3. Inhibitory effect of the peptides on binding of GST-α1 and GST-α2 A domains to their respective collagens. Binding of (A and B) the GST-α1A domain to CB3 (collagen IV fragment); and (C and D) the GST-α2A domain to collagen I in the presence of (A and C) 1 μM; (B and D) 2-1000 μM of the peptides. The solid symbols represent Viperistatin (circles), Rhodocetin (squares), the open symbols represent Compound 6 (circles) and Compound 10 (squares).

Figure 4. Conformational space sampled by Viperistatin (A), Obtustatin (B), Compound 3 (C), Compound 5 (D), Compound 6 (E) and Compound 10 (F). Viperistatin and Obtustatin depicted as "sausage" plots based on the mean structure computed from the last 400 collected conformations superimposed over the backbone of residues 4-18 and 30-36. Atom-wise error bars are indicated by the thickness of the sausages. Compounds 3, 5, 6 and 10 are represented by ten, evenly spread snapshots, taken from within the last 400 snapshots collected during the simulation. Snapshots are shown as solid ribbons with residues of the integrin-recognition motifs (KTS) colored in pink. Disulfide bonds are shown in stick representation.

Figure 5. Conformational similarities between designed and reference compounds (Obtustatin/Viperistatin) calculated by the "contained" analysis. Pie charts represent the

distribution of conformations of the designed compounds within the conformational space of the reference compounds (left) and of the reference compounds within the conformational space of the designed compounds (right). Purple slices represent percentages of conformational ensembles overlapping. Blue and orange slices represent percentages of non-overlapping ensembles. Percentages were calculated as an average over Obtustatin and Viperistatin. (A) Compound 3; (B) Compound 5; (C) Compound 6; (D) Compound 10.

Figure 6. Effect of the peptides on proliferation of endothelial cells. In each experiment A) HAEC and B) HUVEC, 50 μg of peptide per sample were used. Obtustatin served as positive control and proliferation was measured by the BrdU assay. $p^{*}<0.05$ compared with the control.

Figure 7. Inhibitory effect of the peptides on HUVEC migration in wound healing assay. Representative photos of the wounds: zero time (left panel) and 24 h (right panel) from wounding: A) in the absence of the peptides (Control), in the presence of B) 5 μg of Obtustatin, and 50 μg of C) Compound 6, and D) Compound 10.

Figure 8. Inhibitory effect of the peptides on endothelial cell tube formation in the Matrigel assay. Tube formation in Matrigel with A) HAEC and B) HUVEC was induced by complete EBM-2 medium in the absence (negative control) or in the presence of 100 μg of each peptide per sample.

Figure 9. Inhibitory effect of the peptides on VEGF-induced angiogenesis in the Japanese quail CAM model. Representative binary images of mid-arterial end point fragments of CAMs dissected from embryos are presented in the panel: basal level of angiogenesis (Control); angiogenesis induced by 10 μg VEGF/embryo (VEGF); the inhibitory effect of 20 μg

Obtustatin/embryo (Obtustatin), 200 µg/embryo peptides (Compounds 3, 6 and 10) on angiogenesis-induced by 10 µg VEGF. *p<0.001 vs Control. **p<0.001 vs VEGF.

Figure 10. Inhibitory effect of the peptides on glioma LN18 cell-induced angiogenesis in the Japanese quail CAM model. A) Representative binary images of mid-arterial end points fragments of CAMs dissected from embryos appear in the panel: basal level of angiogenesis (Control); angiogenesis induced by LN18 cells (1x107/embryo) (LN18); the inhibitory effect of 100 µg of peptides (Compounds 6 and 10) on angiogenesis induced by LN18. *p<0.001 vs Control. **p<0.001 vs LN18. B) Representative micrographs of dissected CAMs. The tumors are framed in red.

Figure 11. Inhibitory effect of the peptides on bFGF induced angiogenesis in corneal micropocket assay. Upper panel: Newly formed blood vessels are growing toward bFGF pellet (in white); lower panel shows the quantification of neovascularization area in the cornea (n=10, mean ± S.D.). *p<0.05 vs control.

Figure 12. Serum stability profiles of the peptides. Compound 3 (squares), Compound 6 (triangles) and Compound 10 (circles). Relative peptide concentrations were determined by integration of the A_{220} peaks from RP-HPLC chromatograms.

JPET Fast Forward. Published on June 17, 2014 as DOI: 10.1124/jpet.114.214643
This article has not been copyedited and formatted. The final version may differ from this version.

Table 1. Sequence of synthesized linear peptides and their activity.

Amino acid position / Compound	19	20	21	22	23	24	25	26	27	28	29	IC_{50} (mM)
1	**C**	**W**	**K**	**T**	**S**	**L**	**T**	**S**	**H**	**Y**	**C**	0.645
2	**G**	**W**	**K**	**T**	**S**	**L**	**T**	**S**	**H**	**Y**	**G**	> 4
3	**C**	**W**	**K**	**T**	**S**	**R**	**T**	**S**	**H**	**Y**	**C**	0.105
4	**G**	**W**	**K**	**T**	**S**	**R**	**T**	**S**	**H**	**Y**	**G**	3.750

Peptides 1 and 2 are derived from the Obtustatin sequence, Peptides 3 and 4 are Viperistatin analogs. Inhibition of the adhesion of the cells overexpressing α1 integrin measured by IC_{50}.

JPET Fast Forward. Published on June 17, 2014 as DOI: 10.1124/jpet.114.214643
This article has not been copyedited and formatted. The final version may differ from this version.

Table 2. The peptides' potency and efficacy of inhibition of α1 and α2 overexpressor cell's adhesion.

Peptides	α1 overexpressor cells		α2 overexpressor cells	
	Potency IC_{50} (nM)	Efficacy (%)	Potency IC_{50} (nM)	Efficacy (%)
Viperistatin	0.60	100	0	0
Vixapatin	0	0	3.00	100
Compound 5	0.20	20	0.12	10
Compound 6	0.17	20	0.15	30
Compound 7	0.15	25	0.15	25
Compound 8	0.15	25	0.18	20
Compound 9	0.17	40	0.17	10
Compound 10	0.17	40	0.25	20

The values of IC_{50} and efficacy were calculated from the adhesion-log peptide concentration curves, considering zero effect in the absence of the peptide and maximal inhibitory effect at the peptide concentration on which a plateau was measured.

JPET Fast Forward. Published on June 17, 2014 as DOI: 10.1124/jpet.114.214643
This article has not been copyedited and formatted. The final version may differ from this version.

Table 3. Percentages of "contained" conformations. Calculations employed a backbone RMSD cutoff of 2 Å calculated for residues 19-29 and were performed for the last 400 conformations obtained from each simulation.

	Compound 3	Compound 5	Compound 6	Compound 10
Obtustatin				
a	11.5	30.4	3.7	94.5
b	79.6	34.9	50.6	64.3
Viperistatin				
a	17.0	40.1	10.0	94.5
b	96.8	88.0	19.0	68.1

(a) Percentage of the conformational space of the compound contained within the conformational space of Obtustatin and Viperistatin.

(b) Percentage of the conformational space of Obtustatin and Viperistatin contained within the conformational space of the compound.

JPET Fast Forward. Published on June 17, 2014 as DOI: 10.1124/jpet.114.214643
This article has not been copyedited and formatted. The final version may differ from this version.

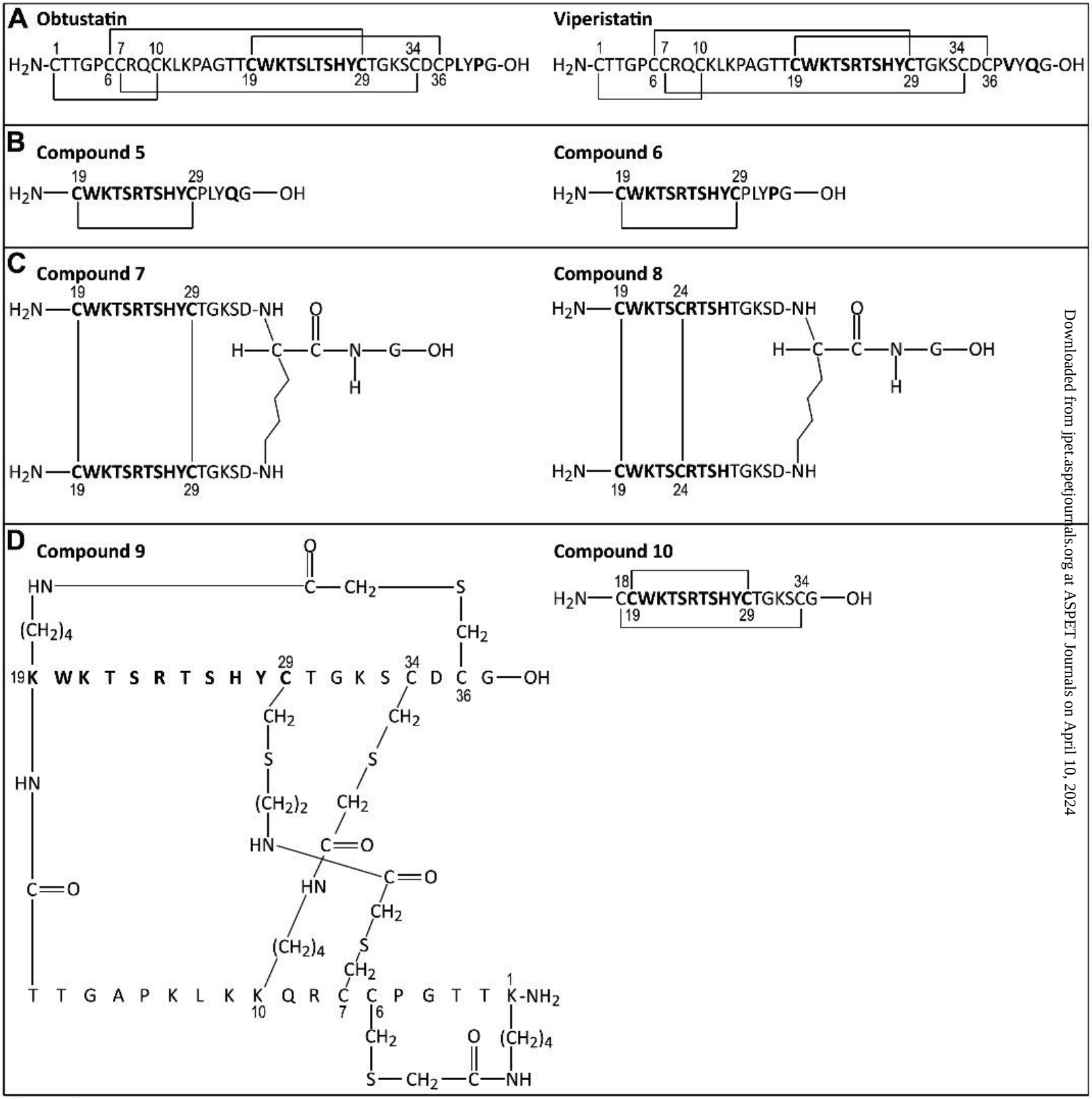

Figure 1

JPET Fast Forward. Published on June 17, 2014 as DOI: 10.1124/jpet.114.214643

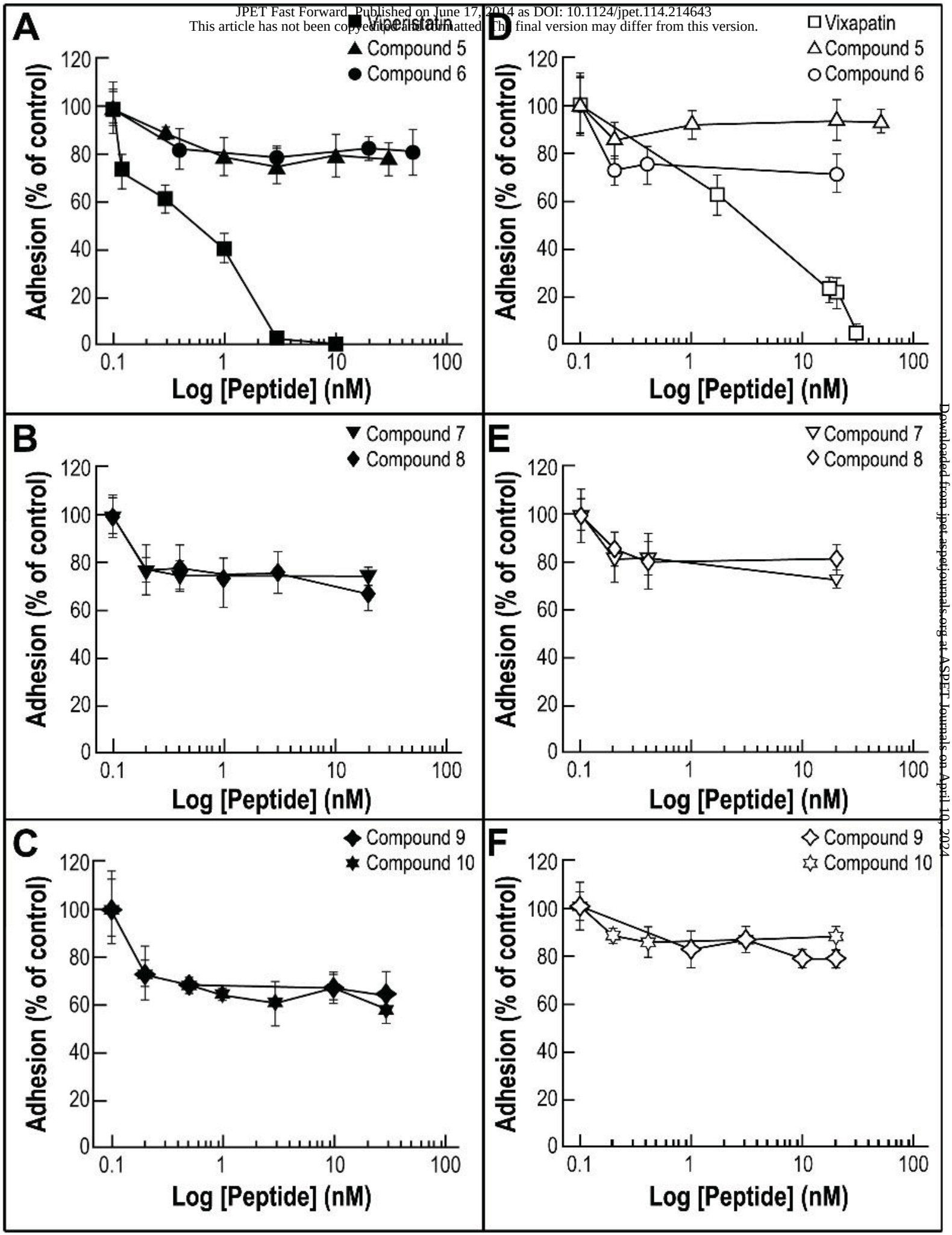

Figure 2

JPET Fast Forward. Published on June 17, 2014 as DOI: 10.1124/jpet.114.214643
This article has not been copyedited and formatted. The final version may differ from this version.

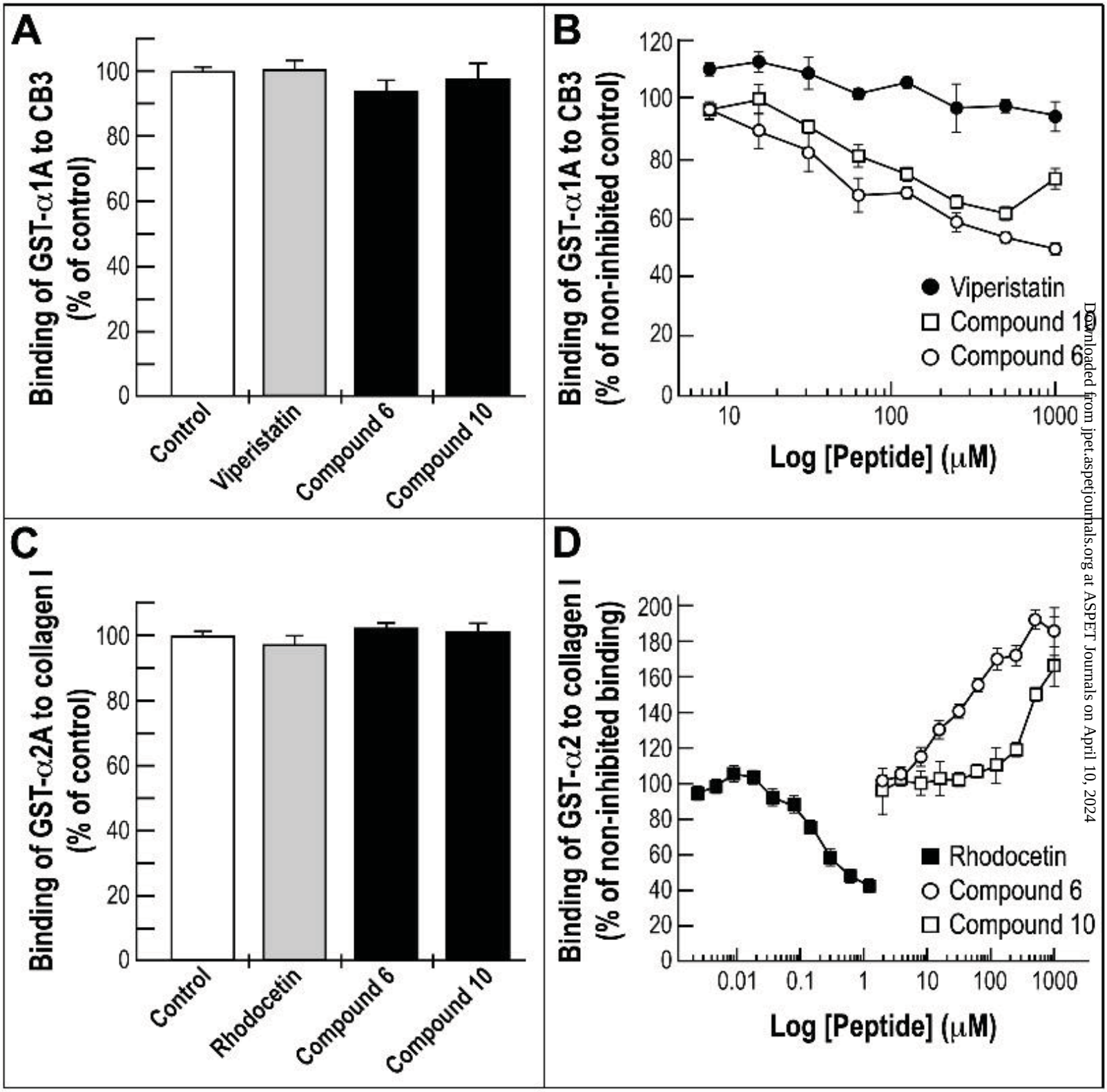

Figure 3

JPET Fast Forward. Published on June 17, 2014 as DOI: 10.1124/jpet.114.214643
This article has not been copyedited and formatted. The final version may differ from this version.

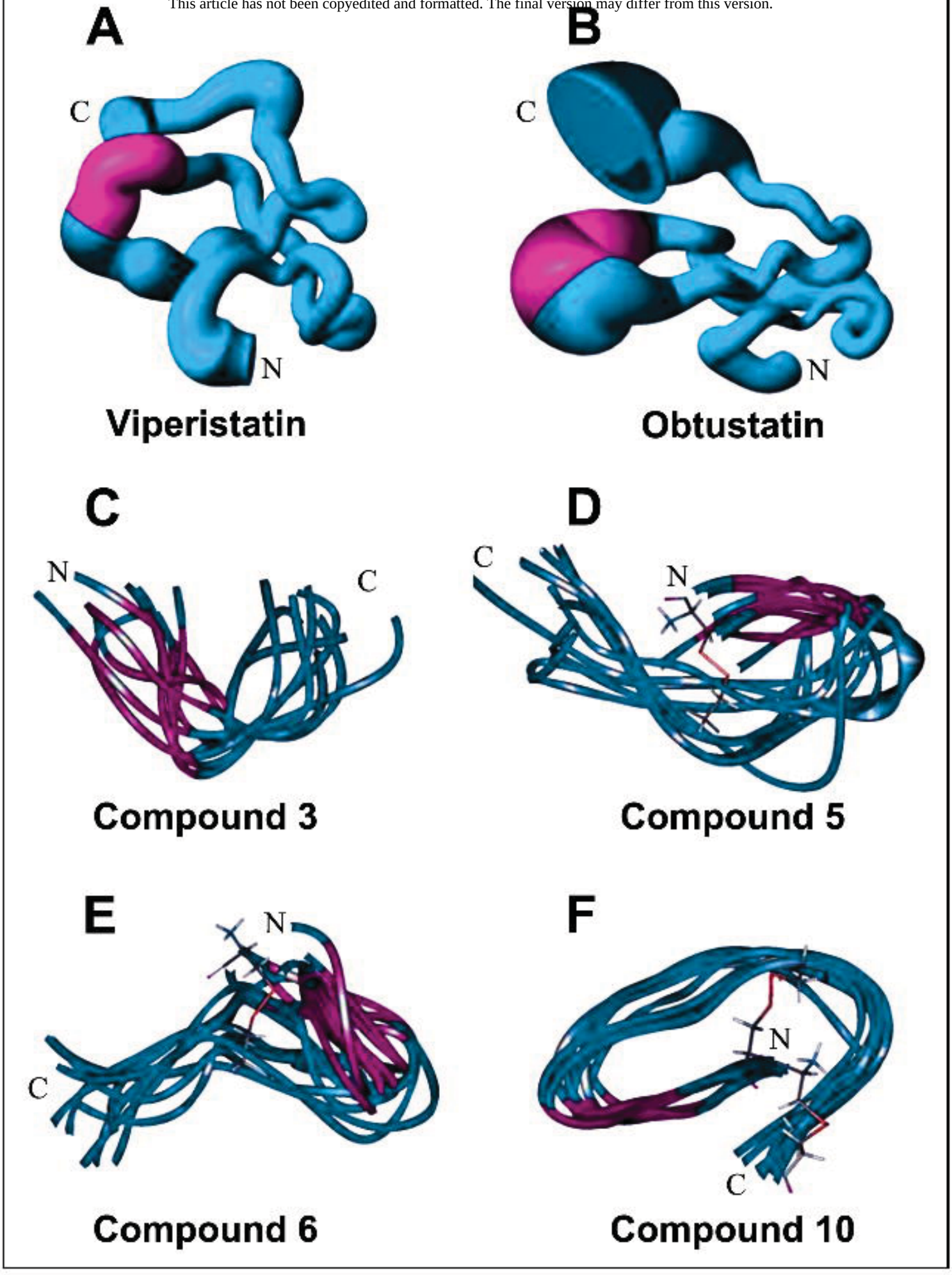

Figure 4

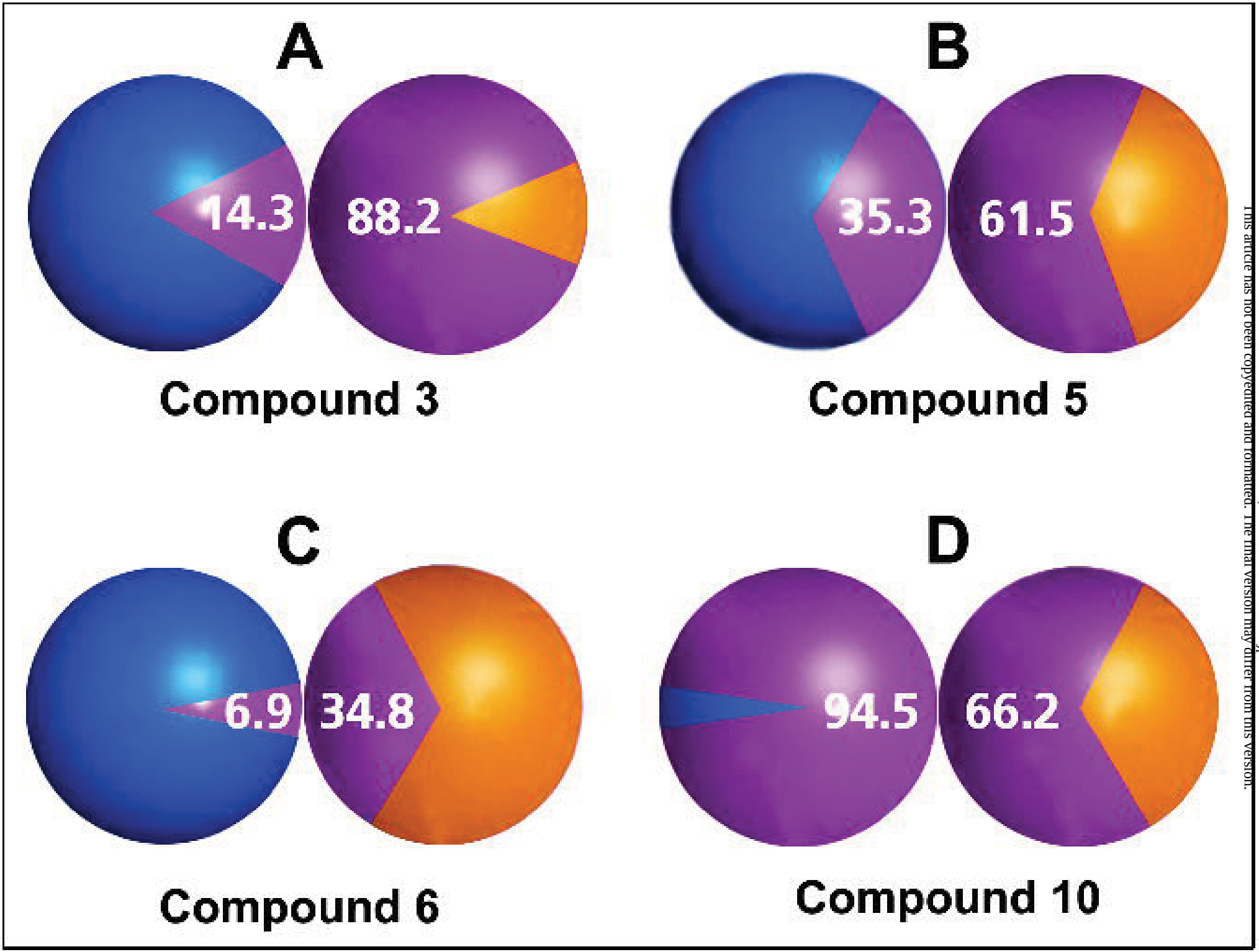

Figure 5

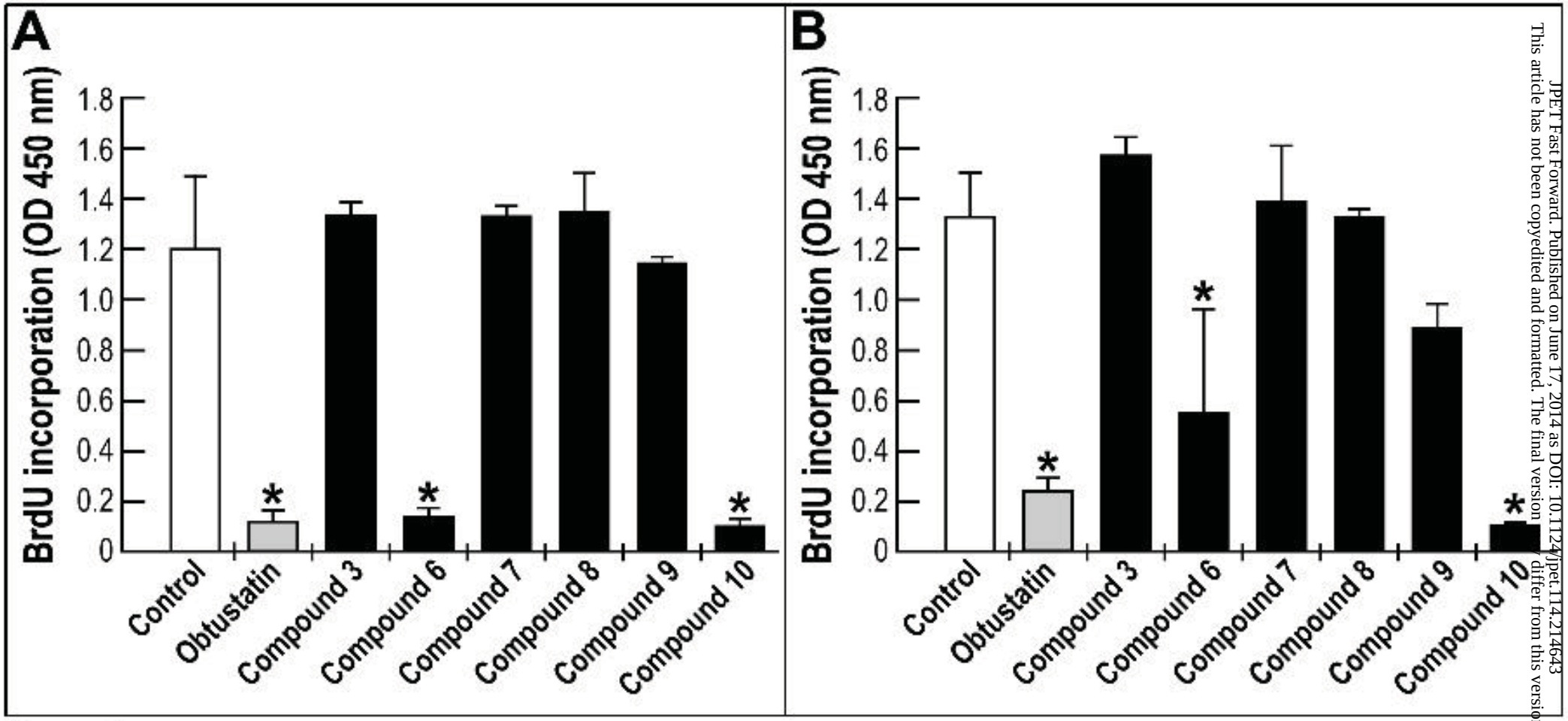

Figure 6

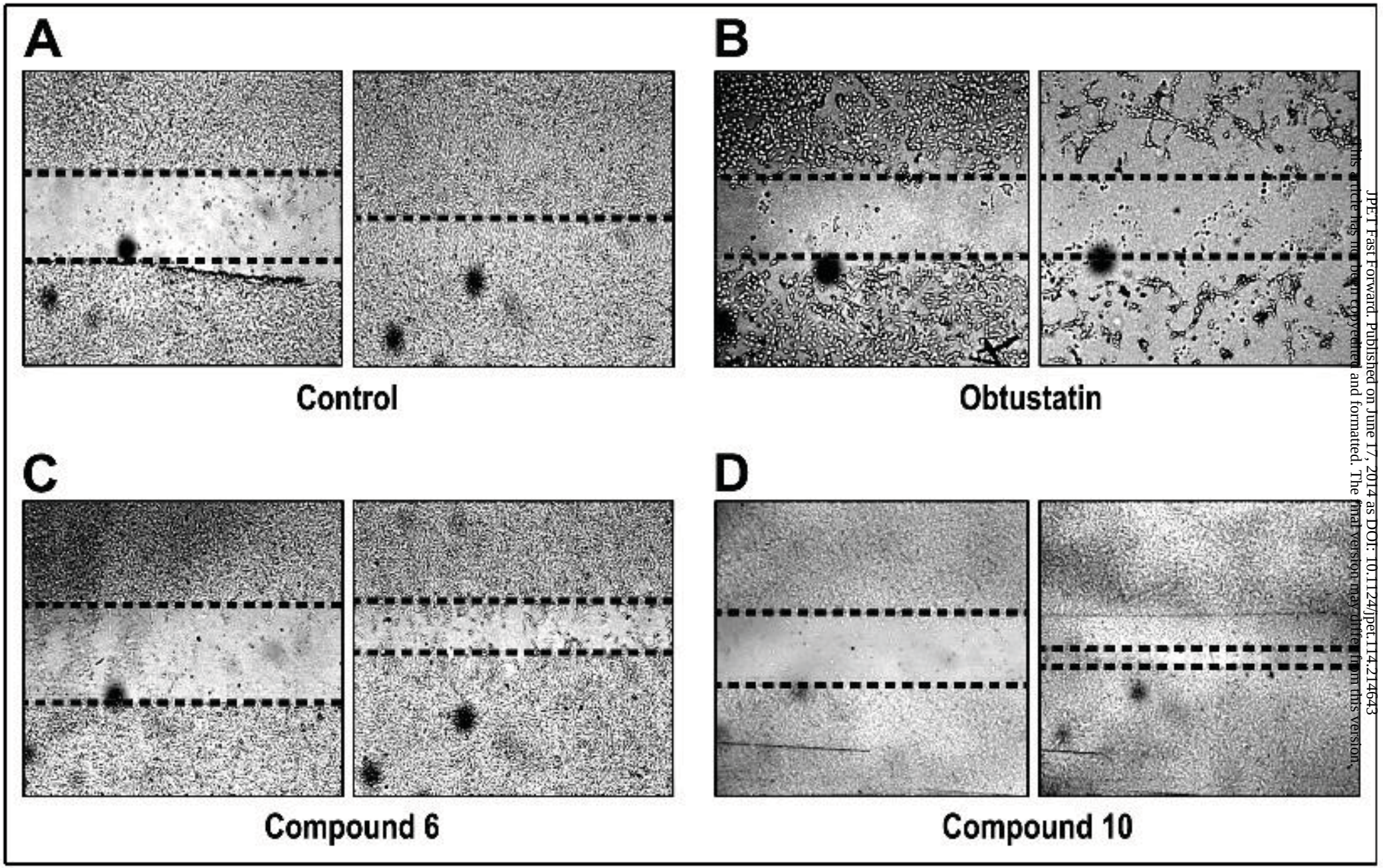

Figure 7

Figure 8

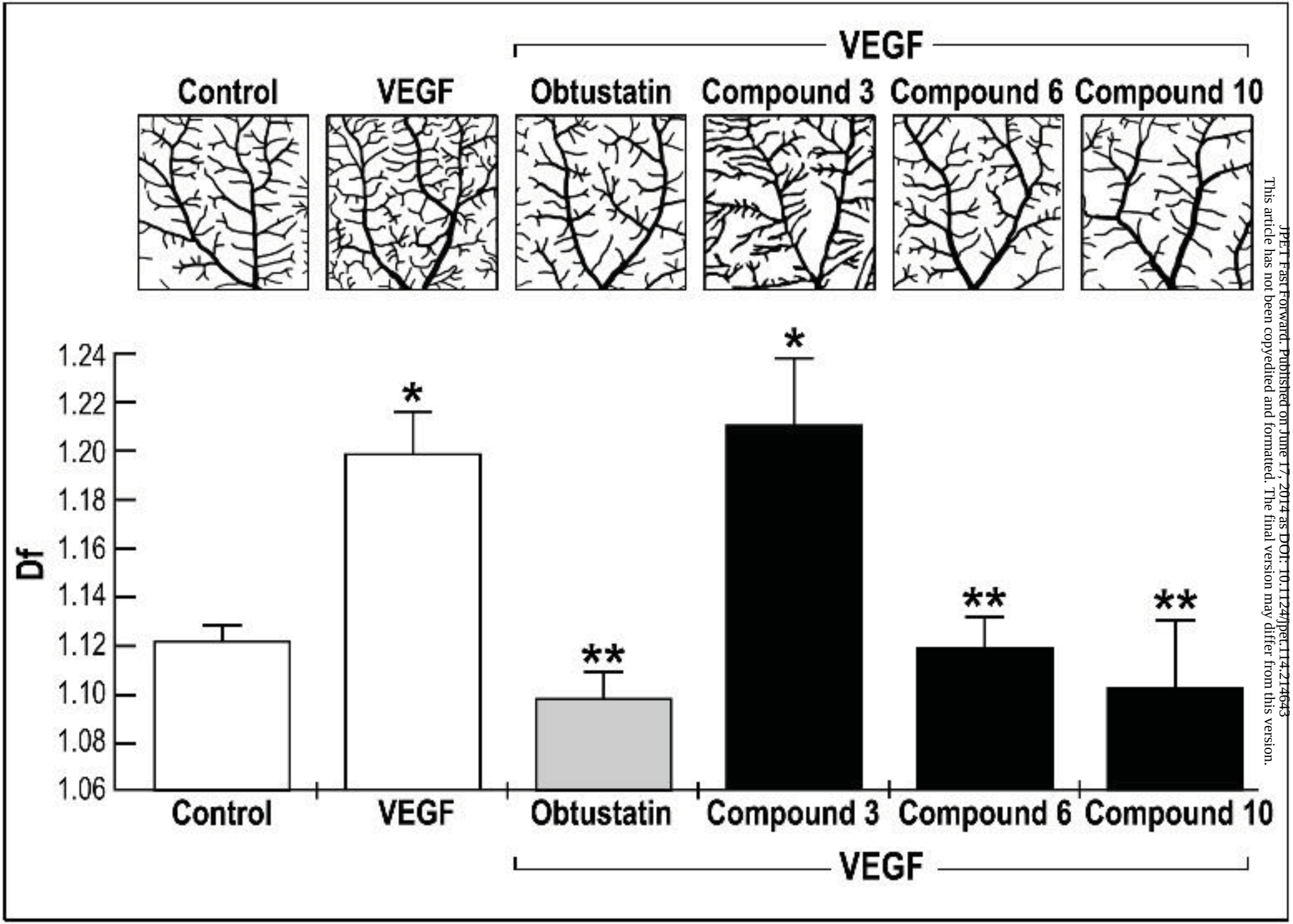

Figure 9

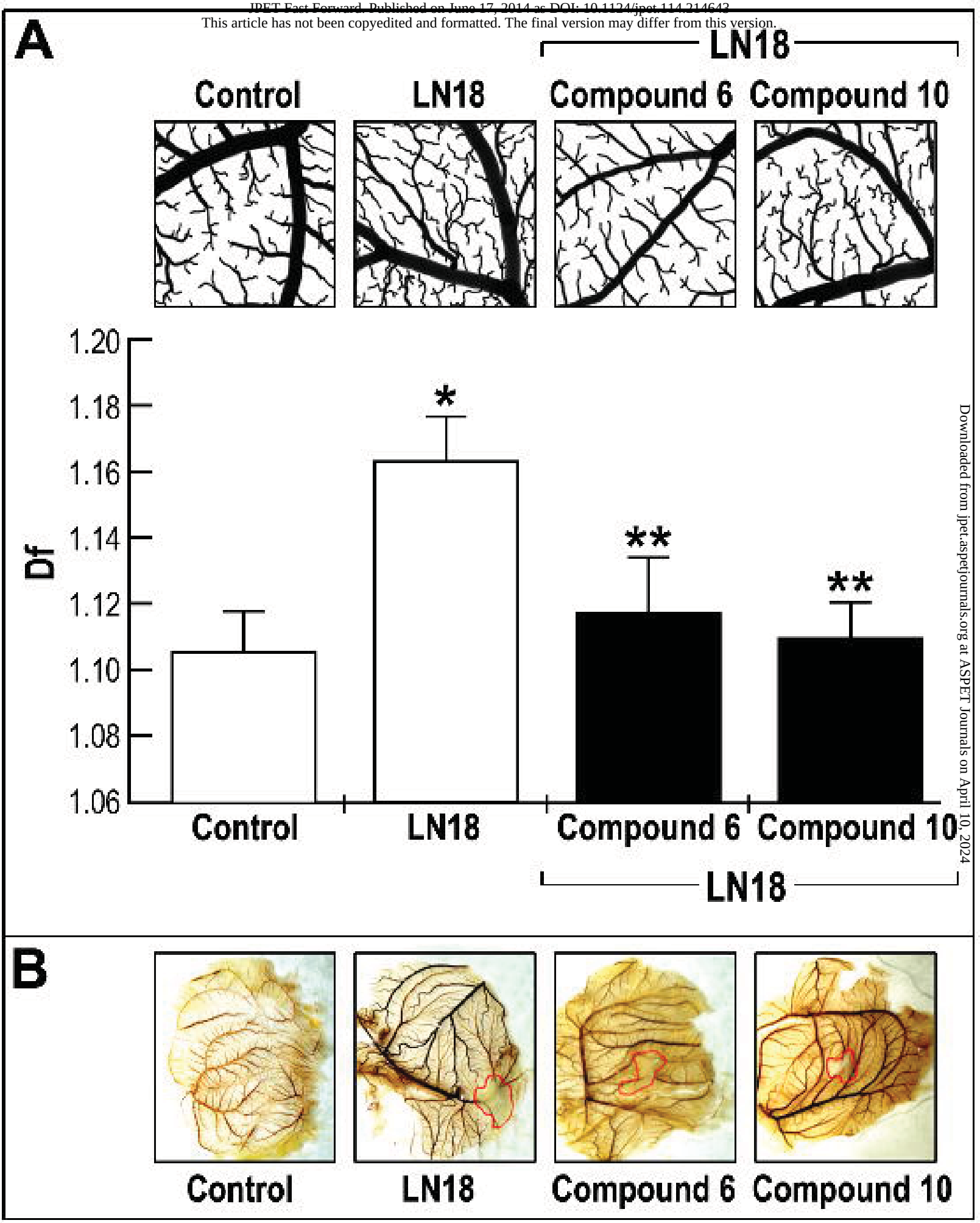

Figure 10

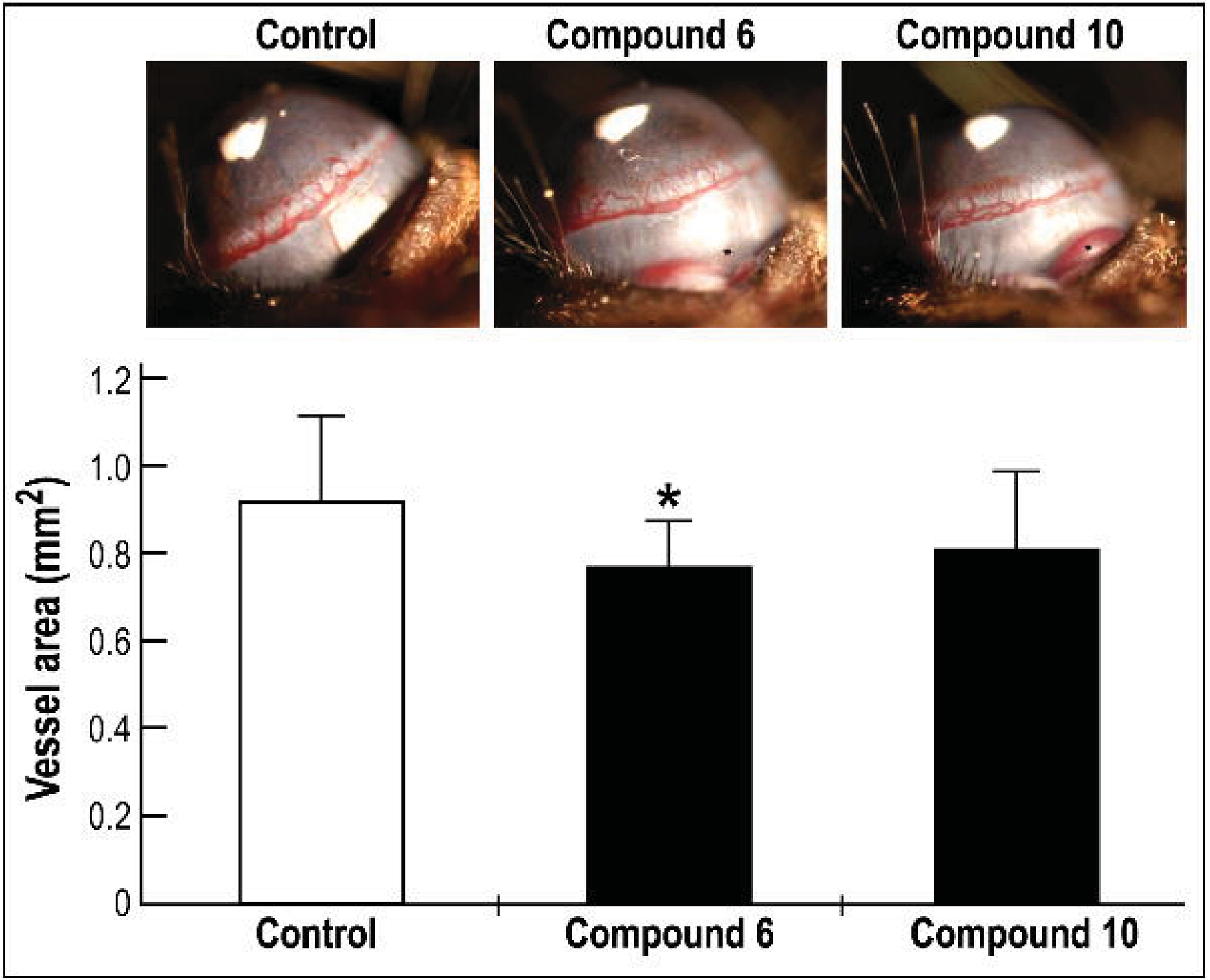

Figure 11

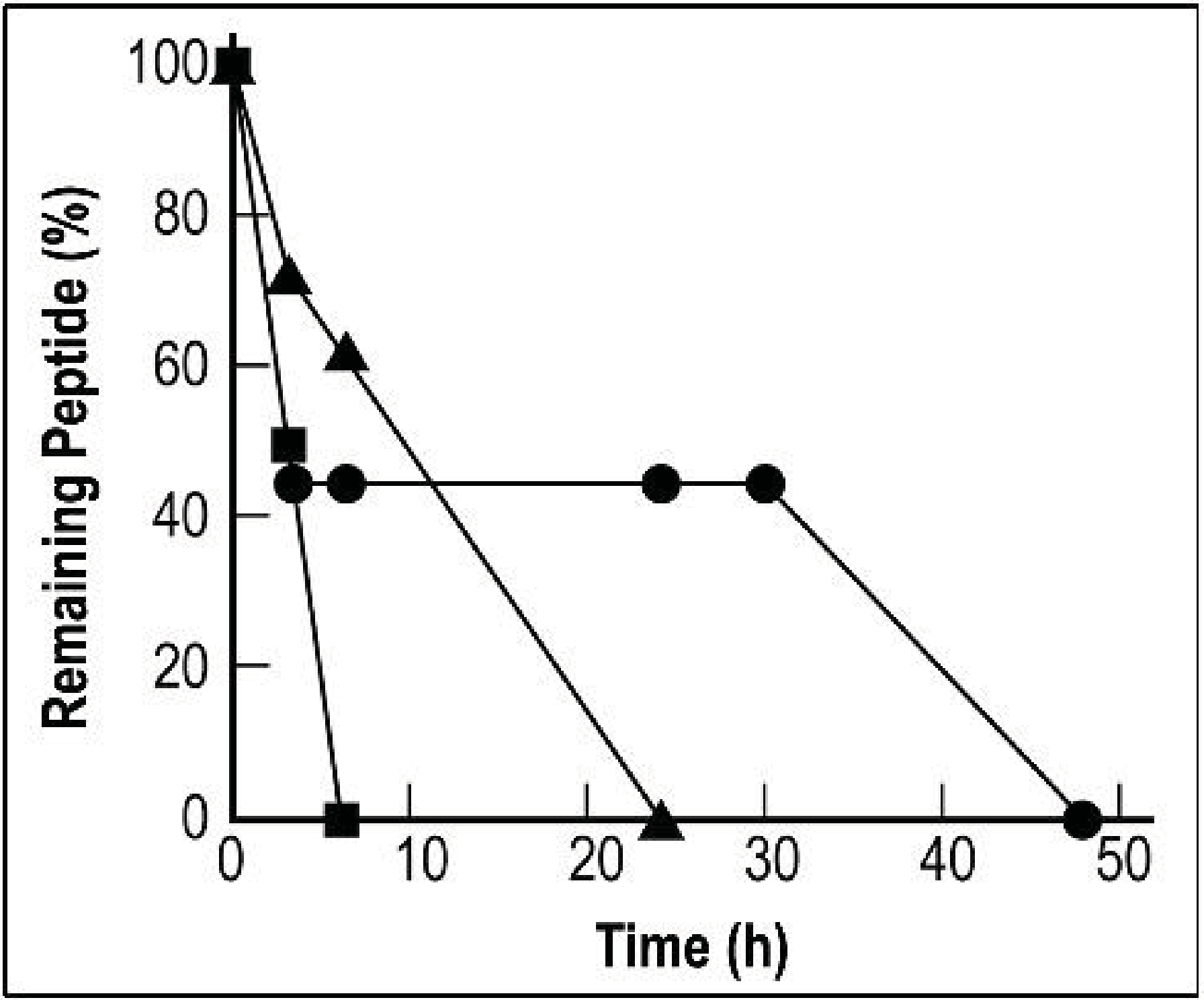

Figure 12